Journal of Experimental Botany, Vol. 70, No. 19 pp. 5071–5088, 2019
doi:10.1093/jxb/erz262 Advance Access Publication August 28, 2019
This paper is available online free of all access charges (see https://academic.oup.com/jxb/pages/openaccess for further details)

RESEARCH PAPER

New steps in mucilage biosynthesis revealed by analysis of the transcriptome of the UDP-rhamnose/UDP-galactose transporter 2 mutant

Juan Pablo Parra-Rojas*, Asier Largo-Gosens*, Tomás Carrasco, Jonathan Celiz-Balboa, Verónica Arenas-Morales, Pablo Sepúlveda-Orellana, Henry Temple, Dayan Sanhueza, Francisca C Reyes, Claudio Meneses, Susana Saez-Aguayo† and Ariel Orellana†

Centro de Biotecnología Vegetal, FONDAP Center for Genome Regulation, Facultad de Ciencias de la Vida, Universidad Andres Bello, Santiago, Chile

*These authors contributed equally to this work.
†Correspondence: aorellana@unab.cl or susana.saez@unab.cl

Received 2 April 2019; Editorial decision 21 May 2019; Accepted 5 May 2019

Editor: Simon Turner, University of Manchester, UK

Abstract

Upon imbibition, epidermal cells of *Arabidopsis thaliana* seeds release a mucilage formed mostly by pectic polysaccharides. The Arabidopsis mucilage is composed mainly of unbranched rhamnogalacturonan-I (RG-I), with low amounts of cellulose, homogalacturonan, and traces of xylan, xyloglucan, galactoglucomannan, and galactan. The pectin-rich composition of the mucilage and their simple extractability makes this structure a good candidate to study the biosynthesis of pectic polysaccharides and their modification. Here, we characterize the mucilage phenotype of a mutant in the UDP-rhamnose/galactose transporter 2 (*URGT2*), which exhibits a reduction in RG-I and also shows pleiotropic changes, suggesting the existence of compensation mechanisms triggered by the lack of URGT2. To gain an insight into the possible compensation mechanisms activated in the mutant, we performed a transcriptome analysis of developing seeds using RNA sequencing (RNA-seq). The results showed a significant misregulation of 3149 genes, 37 of them (out of the 75 genes described to date) encoding genes proposed to be involved in mucilage biosynthesis and/or its modification. The changes observed in *urgt2* included the up-regulation of *UAFT2*, a UDP-arabinofuranose transporter, and *UUAT3*, a paralog of the UDP-uronic acid transporter *UUAT1*, suggesting that they play a role in mucilage biosynthesis. Mutants in both genes showed changes in mucilage composition and structure, confirming their participation in mucilage biosynthesis. Our results suggest that plants lacking a UDP-rhamnose/galactose transporter undergo important changes in gene expression, probably to compensate modifications in the plant cell wall due to the lack of a gene involved in its biosynthesis.

Keywords: Arabidopsis, cell wall, mucilage, nucleotide sugar transporters, seed coat, transcriptome.

Introduction

The plant cell wall is a highly dynamic structure composed of hemicellulose, pectins, proteins, cellulose, and aromatic compounds which surround the cell membrane acting as a physical barrier, influencing plant development, cell morphology and also controlling external environmental cues (Verhertbruggen *et al.*, 2013; Levesque-Tremblay *et al.*, 2015; Rasool *et al.*, 2017;

Wolf et al., 2017). The tight synergistic regulation between the integrity of cell walls and physiological as well as environmental factors comprises the control of a large repertoire of genes involved in cell wall biosynthesis and metabolism (Höfte and Voxeur, 2017; Barnes and Anderson, 2018; Gigli-Bisceglia and Hamann, 2018). Hence, coordinated changes of the cell wall composition and structure allow plants to grow and react to external factors, indicating that cell walls can functionally adapt to respond to new environmental cues. There are other circumstances where plants harbouring mutations in genes involved in the metabolism of the plant cell wall exhibit changes in its structure and composition, triggering the expression of other genes to compensate the changes produced in the mutant in order to maintain cell wall functionality (Burton et al., 2000; Bischoff et al., 2009; Carpita and McCann, 2015; Guénin et al., 2017). In fact, the existence of complex transcriptional regulatory networks, which control the expression of a huge amount of genes related to the synthesis and/or modification of the cell wall, has been described (Yong et al., 2005; Carpita and McCann, 2015; Taylor-Teeples et al., 2015; Golz et al., 2018). Therefore, the study of single cell wall mutants sometimes makes the observation of obvious phenotypes difficult (Carpita and McCann, 2015). Evidence of compensatory mechanisms, leading to the maintenance of cell wall functionality, has been provided in different studies (Burton et al., 2000; Yong et al., 2005; Bischoff et al., 2009; Guénin et al., 2011; Kim et al., 2015; Saez-Aguayo et al., 2017; Xu et al., 2017). In this regard, a recent study by Guénin et al. (2017) comparing the transcriptome from the hypocotyl of etiolated plants from the wild-type and a mutant in pectin methyl esterase 3 (*PME3*), showed a down-regulation of genes coding for pectin-degrading enzymes in the mutant, supporting the hypothesis that connects pectin methylesterification and degradation; however, this mutant also showed an increase in the vacuolar CRUCIFERIN, the most abundant storage protein in Arabidopsis seeds (Guénin et al., 2017). How this result is linked to pectin metabolism remains unclear, but it certainly shows that a mutation in a gene involved in pectin metabolism leads to unexpected changes in gene expression.

Mucilage is an extracellular matrix that has been quite suitable to study pectin biosynthesis and its modification. Seed coat mucilage represents 3% of the seed weight and most of it corresponds to pectin, which is easily extruded from mature dry seed upon imbibition in water (Western et al., 2000; Young et al., 2008; Arsovski et al., 2010; Western, 2012; Francoz et al., 2015). Mutations affecting mucilage composition sometimes do not lead to other physiological effects on the plant, making it a good tool to identify proteins involved in the biosynthesis and modification of pectins (Western et al., 2000; Young et al., 2008; Dean et al., 2011; Western, 2012; Saez-Aguayo et al., 2013; Rautengarten et al., 2014; Francoz et al., 2015; Voiniciuc et al., 2015*b*, *c*; Ralet et al., 2016; Saez-Aguayo et al., 2017; Shi et al., 2018). Mucilage is constituted by soluble (SM) and adherent (AM) layers. Both of them are composed mainly (>90%) of unbranched rhamnogalacturonan 1 (RG-I), a polymer made of alternating repeats of (1,4)-α-D-GalA and (1,2)-α-L-Rha units (Ridley et al., 2001; Ralet et al., 2016). The SM layer can be removed easily upon water imbibition and, in addition to Rha and GalA, it contains traces of Ara, Xyl, Man, Gal, and Glc (Macquet et al., 2007; Voiniciuc et al., 2015*b*, *c*; Ralet et al., 2016). In contrast to the SM, the AM is attached to the seed surface and can be detached from the seed by digestion with rhamnogalacturonan hydrolase (Macquet et al., 2007), by high-speed mechanical agitation (Voiniciuc et al., 2015*c*), or by ultrasonic treatment (Zhao et al., 2017). In addition to RG-I, the AM contains minor amounts of cellulose, arabinan, galactan, galactoglucomannan, and homogalacturonan (HG; Macquet et al., 2007; Voiniciuc et al., 2015*b*; Ralet et al., 2016).

The synthesis of hemicellulose and pectins occurs in the Golgi apparatus, where a number of glycosyltransferases (GTs) transfer the sugar residue from an activated sugar nucleotide donor, UDP- or GDP-sugar, to a growing polysaccharide chain. Most GTs are type-II membrane-bound proteins with a catalytic domain facing the Golgi lumen (Wulff et al., 2000; Sterling et al., 2001; Scheible and Pauly, 2004; Liepman et al., 2010). However, most nucleotide sugars used by GTs are synthesized in the cytosol (Bonin et al., 1997; Seifert, 2004; Bar-Peled and O'Neill, 2011); therefore, the Golgi membrane is a physical barrier blocking the access of UDP/GDP-sugars to the active site of the GTs. To cope with this topological problem, nucleotide sugar transporters (NSTs) located in the Golgi membrane transport UDP/GDP-sugars from the cytosol to the Golgi lumen and supply to the GTs the substrates needed for polysaccharide biosynthesis (Reyes and Orellana, 2008; Orellana et al., 2016; Temple et al., 2016). In *Arabidopsis thaliana*, 44 genes encode putative NSTs and they are similar to those encoding plastidic triose phosphate translocators (TPTs); altogether, they form a gene family of 51 members (Knappe et al., 2003; Rautengarten et al., 2014). To date, a number of these NSTs have been functionally characterized, specifically transporters for GDP-Man, GDP-Fuc, UDP-Gal, UDP-Glc, UDP-Rha, UDP-Xyl, UDP-GalA, UDP-GlcA, and UDP-Araf (Baldwin et al., 2001; Norambuena et al., 2002, 2005; Handford et al., 2004, 2012; Bakker et al., 2005; Rollwitz et al., 2006; Rautengarten et al., 2014, 2016, 2017; Ebert et al., 2015; Saez-Aguayo et al., 2017). Furthermore, more recently *URGT2* and *UUAT1* were characterized as a UDP-rhamnose/UDP-galactose transporter gene and a UDP-uronic acid transporter gene, respectively, and mutations in both genes led to changes in mucilage composition. Both mutants exhibited less Rha and GalA in the SM layer, suggesting that levels of RG-I are affected in mutants in these transporters (Rautengarten et al., 2014; Saez-Aguayo et al., 2017). However, the *urgt2* mutant exhibits a stronger mucilage reduction than the *uuat1* mutant, suggesting the predominant participation of URGT2 in providing substrates to GTs during mucilage RG-I biosynthesis. Interestingly, higher levels of methylesterification of HG were also observed in mucilage from the *uuat1* mutant in comparison with wild-type plants, suggesting the triggering of compensation mechanisms when genes involved in mucilage biosynthesis are mutated (Saez-Aguayo et al., 2017). Since some of the misregulated genes may be directly involved in cell wall biosynthesis, their identification can lead us to discover new players in this process. Therefore, we investigated further the mucilage phenotypes of *urgt2-2* and compared the transcriptomes of both the wild-type (Col-0) and *urgt2-2*. The results revealed several pleiotropic changes

affecting sugar composition and also the organization of seed coat mucilage. In order to identify misregulated genes triggered by the lack of *URGT2* during mucilage production, we performed a comparative transcriptome analysis of developing seeds from wild-type and *urgt2-2* at 8 days after pollination (8 DAP) using RNA sequencing (RNA-seq). The results revealed changes in the expression of 3149 genes during the stages when the mucilage secretory cells are actively engaged in the production of large amounts of pectin. The results also showed that the lack of *URGT2* leads to an up-regulation of genes already described as involved in mucilage biosynthesis. Moreover, we observed changes in the expression of other cell wall-related genes, which can explain some of the phenotypes observed in the mutant. In particular, we found up-regulation of *UAFT2* and *UUAT3*, two genes coding for NSTs not described previously to play a role in mucilage biosynthesis. To confirm their function, we selected mutants and performed biochemical analyses of the mucilage. The results showed that both *uaft2* and *uuat3* exhibited changes in mucilage composition, confirming their role in the biosynthesis of mucilage.

Materials and methods

Plant growth

Arabidopsis thaliana plants were germinated and grown in a growth chamber using a long-day period (16 h photoperiod); the light intensity was 120 mmol m^{-2} s^{-1} and the temperature varied between 19 °C and 28 °C. For collection of seeds and aerial tissue, plants were grown in soil (Top Crop) supplemented with fertilizer (Top Veg) at a relative humidity of 65%. The plants were germinated in Murashige and Skoog (MS) medium (Duchefa) (2.155 g l^{-1}), 1% sucrose, and 0.4% agar. T-DNA insertion lines for *urgt2-1* (SALK_125196), *urgt2-2* (SALK_071647), *uaft2-1* (SALK_011583), *uaft2-2* (SALK_018646), and *uuat3-1* (GK-380D03) were obtained from the ABRC (http://abrc.osu.edu/) using the SIGnAL Salk collection (Alonso *et al.*, 2003).

Tissue collection, RNA isolation, and RNA sequencing

Col-0 and *urgt2-2* plants were grown simultaneously under the growth conditions detailed above. Flowers were tagged at the beginning of pollination, which was defined phenotypically as the time at which the flowers were just starting to open, as previously described by Western *et al.* (2000). For RNA-seq experiments, developing seeds were dissected from the siliques at 8 DAP and total RNA was isolated from the developing seeds of four siliques using the RNeasy Plant Micro kit (Qiagen) including a DNase I treatment (Invitrogen™) following the manufacturer's instructions. Samples to make the libraries were obtained from three different plants in order to generate biological replicates. Each total RNA sample had a 260:280 nm ratio of at least 1.8 and an RNA quality number (RQN) value >8.0. From 1.0 µg of total RNA, cDNA libraries for each sample were constructed using the TruSeq® Stranded mRNA kit (Illumina). Quality control and concentration were determined by capillary electrophoresis (Fragment Analyzer®, AATI). Six cDNA libraries (2 genotypes×3 biological replicates) were sequenced on one lane of Illumina NexSeq500.

Cloning procedures

The *URGT2* coding sequence (CDS), without the stop codon, was amplified from cDNA prepared from Arabidopsis leaf RNA, using the primers sense 5'-CACCATGGAGAAAGCAGAGAACGAGA-3' and antisense 5'-TGCTTTATTATTTCCAAGCTCCAT-3'. The resulting PCR products were introduced into the pENTR™/D TOPO® vector according to standard protocols (Life Technologies) to generate the entry clone pENTR-URGT2. The *URGT2* promoter (pURGT2) was amplified from Arabidopsis genomic DNA using the primers 5'-CACCTC ATGTGTTGCGAATCTTATTC-3' and 5'-TTGGATTCAAATTAA AAAAATTCGAAATCTGAAATC-3'. The resultant PCR product was introduced into the pENTR 5-TOPO vector (Thermo Fisher Scientific) to generate the pENTR5-URGT2 entry clone. The C-terminal green fluorescent protein (GFP) fusion was obtained by recombining the entry clone with the destination vector R4pGWB504 (Nakagawa *et al.*, 2007) using LR clonase (Thermo Fisher Scientific).

The entire CDS of the *UUAT3* gene was cloned from cDNA prepared from Arabidopsis leaf RNA. The sequence without the stop codon was PCR-amplified using the following primers: sense 5'-CACCATGAAGATGGCGACGAATGGC-3' and antisense 5'-ATTTTTGTTTCGTTTCTTGGCTTC-3'. The resulting PCR products were introduced as explained above to generate the entry clone pENTR-UUAT3. The intergenic region (1900 bp) between At5g05820 and At5g05830 was defined as the UUAT3 promoter (pUUAT3) and was amplified from Arabidopsis genomic DNA using the following primers: sense 5'-CGCTTTTCTTCTTCCTAATCCTG-3' and antisense 5'- GCCACTGGGTTTTGGAGTTA-3'. The resultant PCR products were introduced into the pENTR™/5'-TOPO® vector (Thermo Fisher Scientific) to generate the pENTR5-pUUAT3. The C-terminal GFP fusion was obtained by recombining the entry clones with the destination vector R4pGWB504 (Nakagawa *et al.*, 2007) using LR clonase (Thermo Fisher Scientific).

Analysis of RNA-sequencing

Raw data reads (.fastq files) were trimmed using the Trim Galore Cutadapt (Martin *et al.*, 2011) wrapper using the -paired and -q 25 option. Trimmed reads were aligned against the Tair10 reference genome (Arabidopsis Genome Initiative, 2000) using STAR (Dobin *et al.*, 2013). Mapped read pair counts were calculated with HTseq-count (Anders *et al.*, 2015) and counts were normalized into CPM (Glusman *et al.*, 2013). Analysis of differentially expressed genes (DEGs) was performed using edgeR (Robinson *et al.*, 2010) considering a false discovery rate (FDR) <0.05, and up-regulated and down-regulated genes were used to identify enriched Gene Ontology terms using AgriGO (Du *et al.*, 2010).

Ruthenium red staining

Mucilage released from mature dry seeds was stained directly with 0.01% (w/v) Ruthenium red after imbibition in 0.5 M EDTA, pH 8.0, for 60 min. The coloration of AM seeds was observed with a stereoscopic microscope (LEICA EZ4 HD).

Seed immunolabeling

Immunolabeling was performed using four monoclonal antibodies, INRA RU1 (recognizes unbranched RG-I), JIM5 (recognizes poorly methylesterified HG), JIM7 (recognizes highly methylesterified HG), and LM25 (recognizes xyloglucan) (Ralet *et al.*, 2010; Saez-Aguayo *et al.*, 2013, 2017). Double labeling with an antibody plus calcofluor white (0.01%, w/v) or propidium iodide (20 mg ml^{-1}) was performed as indicated for each antibody to observe the seed surface and AM layer. Optical sections were obtained using a Leica TCS LSI spectral confocal laser scanning microscope. A 488 nm argon laser line was used to excite Alexa Fluor 488, a 405 nm diode laser line was used to excite calcofluor white, and a 543 nm neon laser line was used to excite propidium iodide. Fluorescence emission was detected between 504 nm and 579 nm for Alexa Fluor 488, between 412 nm and 490 nm for calcofluor white, and between 550 nm and 725 nm for propidium iodide. For comparisons of the signal intensity within one experiment, the laser gain values were fixed.

Extraction of mucilage layers

To determine the monosaccharide contents from SM, AM, and naked seeds, a sequential extraction procedure was carried out. Soluble mucilage was extracted by incubating 50 mg of seeds with 5 ml of water for 3 h.

The adherent layer was detached from the seed by sonication employing an ultrasonic homogenizer sonic ruptor 250 (Omni International©) for 2 min at 20% ultrasonic power followed by 1 min at 30% ultrasonic power. Upon SM and AM extraction, samples were stabilized by heating at 100 °C for 5 min and lyophilized.

AIR preparation and acid hydrolysis

Naked seeds were ground with liquid nitrogen and then washed three times with 80% ethanol (4 h, at room temperature), twice with methanol/chloroform 1/1 (v/v) (3 h, room temperature), and twice with acetone (1 h, room temperature) for removal of lipids. The final acid-insoluble residue (AIR) was dried out overnight at room temperature. Naked seed AIR and mucilage fractions were hydrolyzed for 30 min with 400 µl of 2 M trifluoroacetic acid (TFA) at 121 °C. TFA was evaporated at 65 °C with gaseous nitrogen and the samples were washed twice in 400 µl of 100% isopropanol and dried with gaseous nitrogen. Hydrolyzed products were suspended with water and clarified by passing through a syringe filter (pore size: 0.45 mm), transferred to a new tube, and used for HPAEC-PAD analysis as described below. Inositol and allose were used as internal controls for TFA hydrolysis.

HPAEC-PAD

A Dionex ICS3000 ion chromatography system, equipped with a pulsed amperometric detector, a CarboPac PA1 (4×250 mm) analytical column, and a CarboPac PA1 (4×50 mm) guard column, was used to quantify sugars. The separation of neutral sugars was performed at 26 °C with a flow rate of 1 ml min^{-1} using an isocratic gradient of 20 mM NaOH for 32 min followed by a separation of acidic sugars using 75 mM NaOAc and 150 mM NaOH for 18 min at a flow rate of 1 ml min^{-1} at 26 °C, followed by a wash with 200 mM NaOH for 5 min. After every run, the column was equilibrated in 20 mM NaOH for 10 min. Standard curves of neutral sugars (D-Fuc, L-Rha, L-Ara, D-Gal, D-Glc, D-Xyl, and D-Man) or acidic sugars (D-GalA and D-GlcA) were used for quantification.

Determination of PME activity

Total protein extracts were obtained by grinding 100 mg of dry seeds with extraction buffer (1 M NaCl, 12.5 mM citric acid, and 50 mM Na_2HPO_4, pH 6.5). The resulting homogenate was shaken for 1 h at 4 °C and then centrifuged at 14 000 rpm for 15 min, and the supernatant was retained. Protein concentrations were determined using the BCA kit (Pierce™ BCA Protein Assay Kit, Thermo Scientific), and equal quantities of protein (30 µg) in the same volume (20 µl) were loaded into 6 mm diameter wells in gels prepared with 0.1% (w/v) of 85% esterified citrus fruit pectin (Sigma-Aldrich), 1% (w/v) agarose, 12.5 mM citric acid, and 50 mM Na_2HPO_4 pH 6.5. After incubation overnight at 28 °C, plates were stained with 500 µg ml^{-1} ruthenium red for 45 min and destained with water for >3 h. Measurements of stained areas were performed with ImageJ 1.34S software (Freeware, National Institute of Health).

Methylesterification analysis of mucilage layers and AIR samples

The degree of methylesterification of SM, AM, and naked seeds was measured from methanol released by alkaline de-esterification of extracts with 0.2 M NaOH (for mucilage layers) and with 1 M NaOH (for naked seeds) for 1 h at 4 °C. After the neutralization of extracts with 0.2 M or 1 M HCl, released methanol was measured as described by Saez-Aguayo *et al.* (2013). All experiments were done using five technical replicates and at least three biological replicates.

Expression analysis by quantitative real-time PCR (qRT-PCR)

Seeds were dissected from approximately four siliques at each DAP (6, 8, 10, and 12 DAP) for further RNA extraction. RNA extractions were performed as described above using an RNeasy Plus Micro Kit (Qiagen). A 1 µg aliquot of total RNA was used as a template for first-strand cDNA synthesis with an oligo(dT) primer and SuperScript II (Thermo Fisher Scientific), according to the manufacturer's instructions. For reverse transcription–PCR (RT–PCR) analysis, primers described in Supplementary Table S6 at *JXB* online were used to amplify the entire CDS of *URGT2* from single-stranded cDNA in the WT Col-0, *urgt2-1*, and *urgt2-2*. The primers used to amplify *EF1αA4* were those described by North *et al.* (2007). qRT-PCR was performed using the Fast EvaGreen qPCR Master Mix kit (Mx3000P; Stratagene). Reactions contained 1 µl of 1:2 diluted cDNA in a total volume of 10 µl. Reactions were performed using primers that have been previously tested for their efficiency rates and sensitivity in a cDNA dilution series.

Relative expression

The quantification and normalization procedures were done using the following equation, as described by Stratagene:

$$\text{Releative Expression} = \frac{(1+\text{E target})^{-\Delta \text{Ct target}}}{\sqrt{\left[(1+\text{E Norm1})^{-\Delta \text{Ct Norm1}}\right] \times \left[(1+\text{E Norm2})^{-\Delta \text{Ct Norm2}}\right]}}$$

where E corresponds to the efficiency of amplification of target and reference genes, Ct is the threshold cycle, and Norm1 and Norm2 refer to the references or normalizer genes. *EF1αA4*, and the seed reference gene *At4g12590* (Hong *et al.*, 2010) were used as reference genes, and all primers used in this study are described in Supplementary Table S6.

Results

urgt2-2 *is a knockout mutant affected in mucilage RG-I composition*

The allelic mutants *urgt2-1* and *urgt2-2* mutated in *URGT2* were described by Rautengarten *et al.* (2014), exhibiting a reduction of ~25% and 50% in Rha and GalA content in SM, suggesting that the content of RG-I was compromised (Rautengarten *et al.*, 2014). RT–PCR and qRT-PCR analysis confirmed that both allelic mutants are knockout (Fig. 1B, C; Supplementary Fig. S3A, B), however *urgt2-2* exhibited the greatest changes in mucilage composition (Rautengarten *et al.*, 2014). The monosaccharide composition of both soluble and adherent layers showed that the mutation in *URGT2* affects mucilage composition in both layers with a slight decrease in GalA content in the total sugar mucilage amount (Supplementary Fig. S2A). The molecular rescue of the *urgt2-2* mutant was obtained by transformation with the *proURGT2:URGT2-GFP* construct. Several independent transformants were obtained, and GalA and Rha contents of the SM layer of three independent lines were determined. Contents similar to WT Col-0 plants were obtained for both sugars (Fig. 1D), indicating that *proURGT2:URGT2-GFP* had successfully rescued the mutant. All these results confirm that URGT2 plays a role in SM and AM RG-I biosynthesis.

Transcriptome analyses in developing seeds from wild-type and urgt2-2 *plants*

Since the mutation in *URGT2* can produce changes in the transcriptome from developing seeds as part of possible compensatory mechanisms, we compared the transcriptome of developing seeds from WT Col-0 and *urgt2-2* plants by performing

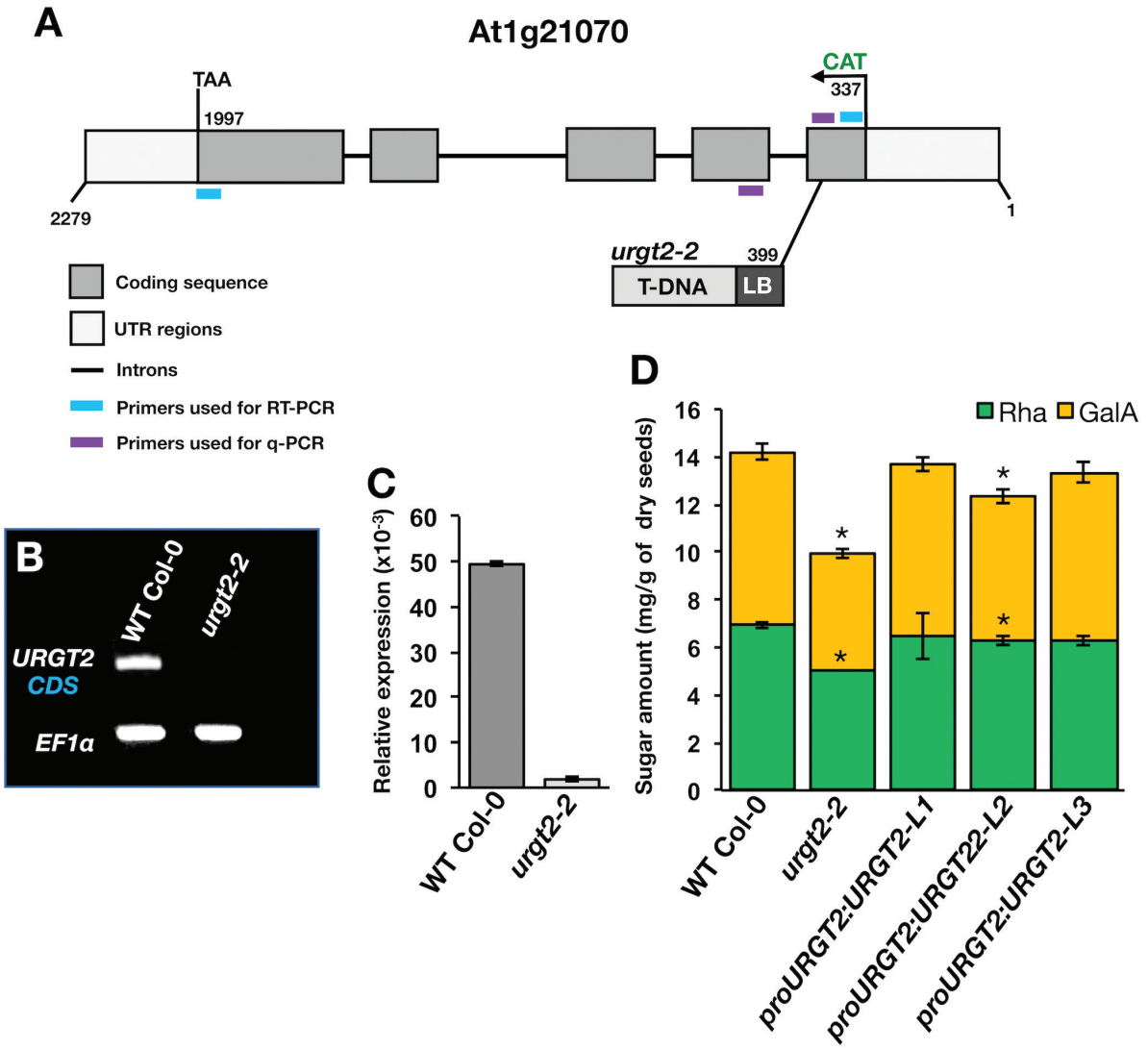

Fig. 1. *urgt2-2* is a knockout line. (A) Schematic representation of *URGT2* structure, as annotated in TAIR (http://www.arabidopsis.org/). The site and orientation of the T-DNA insertion *urgt2-2* allelic line are indicated in the scheme. Numbers indicate the positions (in bp) of the start and stop codons and the T-DNA insertion site. Untranslated regions (light gray boxes), protein coding sequences (dark gray), black lines (introns), and LB (left border) are indicated.(B) Analysis of *URGT2* expression in the *urgt2-2* mutant line. RT–PCR analyses were performed on RNAs isolated from 8 DAP developing seeds from the WT Col-0 and *urgt2-2* line using specific primers for the full-length coding sequence of *URGT2*. *EF1αA4* expression was used as a reference gene. (C) qRT–PCR analysis of *URGT2* transcript steady-state levels in developing seeds in 8 DAP developing seeds from the WT Col-0 and *urgt2-2* mutant line. The expression was calculated relative to *EF1αA4* and a seed-specific reference gene (At4g12590). Error bars represent SE values from three biological replicates (n=9). (D) Rescue of the *urgt2-2* mutant phenotype using the *proURGT2*:*URGT2*-GFP construct. Soluble mucilage content of the WT Col-0, *urgt2-2*, and the transgenic lines *proURGT2*:*URGT2* L1, L2, and L3. The Rha and GalA content was quantified using HPAEC-PAD. Error bars represent SE values from four technical repeats from three independent lines (n=12). Asterisks indicate significant statistical differences using student t-test (*P<0.01).

RNA-seq analyses. To perform the experiment, we looked for the time with the highest expression of *URGT2*; therefore, to determine the moment to collect the seeds for RNA extraction, we determined the *URGT2* expression *in planta* by qRT-PCR (Supplementary Fig. S1). The results showed that *URGT2* is highly expressed in developing seeds at 8 DAP, which corresponds to the stage when mucilage is highly produced and accumulated in the seed coat epidermal cells (Western *et al.*, 2004; Macquet *et al.*, 2007). The results also showed a high expression of *URGT2* in rosettes; however, no phenotype was observed in this tissue. Based on these results, we isolated RNA from developing seeds at 8 DAP from WT Col-0 and *urgt2-2* plants using three biological replicates, and transcriptomic analyses using RNA-seq were performed. We obtained a total of 174 908 519 reads with an average of 29 151 420 reads on each replicate and a minimum and maximum of 24 839 927 and 37 606 112, respectively (Supplementary Table S1). Reads were mapped against the reference genome obtaining 90.2% of mapped reads. Our transcriptomic analysis identified 3149 DEGs between the mutant and the WT Col-0 (FDR <0.01), where 656 were down-regulated and 2493 were up-regulated in *urgt2-2*. Among the 3149 misregulated genes in *urgt2-2*, 168 genes encoded proteins predicted to be involved in cell wall biosynthesis and/or modification (Supplementary Table S2).

To validate the expression pattern obtained by the transcriptomic analysis using RNA-seq, qRT-PCR was carried

out for three genes showing higher abundance in the mutant (*URGT4*/At4g39390, *UUAT1*/At5g04160, and *PME58*/At5g40180) and three genes showing lower abundance in the mutant (*EXPA1*/At1G69530, *XTH8*/At1G11545, and *PME53*/At5g19730) in *urgt2-2*. The analysis of the expression of those genes in developing seed at 8 DAP revealed that both qRT-PCR and RNA-seq analysis had the same change of expression trend when *urgt2-2* expression was compared with the WT Col-0. Therefore, these results validated the strength of the RNA-seq analysis performed on the *urgt2-2* mutant (Fig. 2).

High global changes in specific mucilage genes

To demonstrate the occurrence of possible compensation mechanisms that take place in *urgt2-2* during mucilage biosynthesis and/or modification, we analyzed the expression profile of genes with a known function in this process. To date, 75 genes acting on epidermal cell differentiation, mucilage biosynthesis, mucilage stabilization, hormone synthesis/perception, mucilage secretion, and mucilage modification have been proposed to play a role (Supplementary Table S7; Kong *et al.*, 2013; Rautengarten *et al.*, 2014; Francoz *et al.*, 2015; Voiniciuc et al., 2015*a*, *b*, 2018; Ehlers *et al.*, 2016; Ezquer *et al.*, 2016; Hu *et al.*, 2016; Ralet *et al.*, 2016; Turbant *et al.*, 2016; Griffiths *et al.*, 2017; Saez-Aguayo *et al.*, 2017; Salem *et al.*, 2017; Tsai *et al.*, 2017; Shi *et al.*, 2018; Shimada *et al.*, 2018; Takenaka *et al.*, 2018). From these 75 genes, 37 were differentially expressed in the developing seeds from the WT Col-0 and *urgt2-2* mutants. Interestingly, 35 genes were up-regulated in the mutant (Fig. 3). This differential expression affects genes classified as involved in 'mucilage synthesis' (i.e. *RRT1*, *GATL5*, *GAUT11*, *MUCI70*, *MUM4/RHM2*, *MUCI10*, *IRX7/FRA8*, *MUCI21/MUM5*, *IRX14*, *UUAT1*, and *CSLA2* among others), 'mucilage modification' (i.e. *PMEI6*, *PMEI14*, *ADK1*, *FLY1*, *BLX1*, *MUM2*, and *PME58*), and 'cell wall synthesis and modification' (i.e. *CESA10*, *PRX36/PER36*, *CESA3/IRX1*, and *SBT1.7/ARA12*). We also observed changes in genes involved in transcriptional pathways (*GL2*, *TTG2*, *SHP2*, *MYB5*, and *STK*), mucilage stabilization (*COBL2* and *MUM3/CESA5*), hormone perception (*RAPTOR1B* and *GA1*), and genes affecting mucilage secretion, release, or formation (*TBA2*, *MOR1*, *PRX56*, *SKD1*, and *DRC*). All these changes in the transcriptome suggest that in order to balance the lack of *URGT2*, a deep reorganization takes place, leading to changes in the structure and composition of polymers present in mucilage in the mutant.

Mucilage from urgt2-2 *is not only altered in RG-I monosaccharide composition*

To determine whether the changes observed in the transcriptome led to evident changes in mucilage composition, we carried out biochemical and immunological analyses of both SM and AM fractions. First, we analyzed the monosaccharide

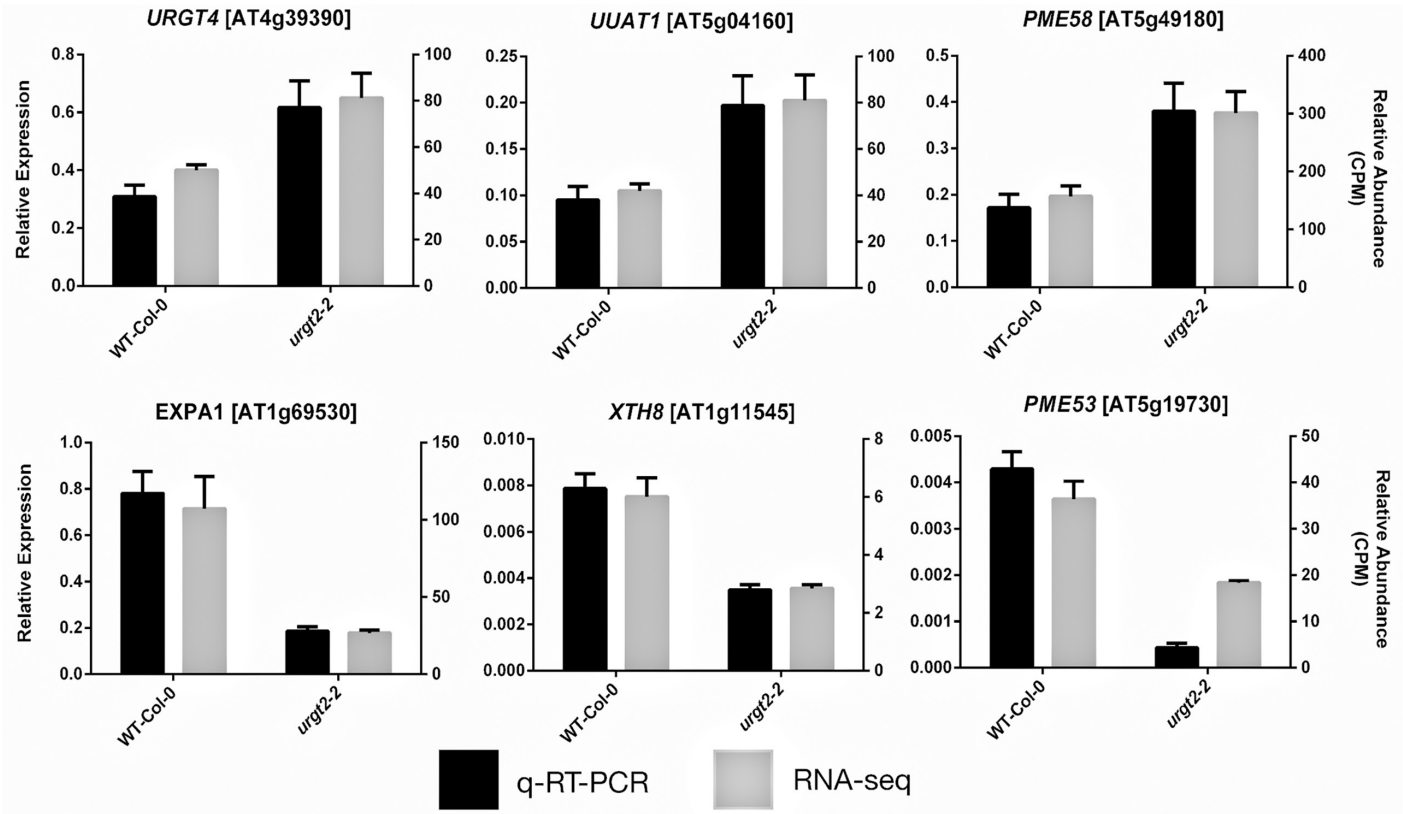

Fig. 2. qRT-PCR validation of the RNA-sequencing (RNA-seq) experiment. Gene expression patterns from the RNA-seq analysis (in gray) were validated for six representative genes by qRT–PCR (in black). The confirmation includes three genes overexpressed (*URGT4*/At4g39390, *UUAT1*/At5g04160, and *PME58*/At5g40180) and three genes repressed (*EXPA1*/At1G69530, *XTH8*/At1G11545, and *PME53*/At5g19730) in the *urgt2-2* mutants, in comparison with the WT Col-0. Error bars represent SE values from three biological replicates (n=9).

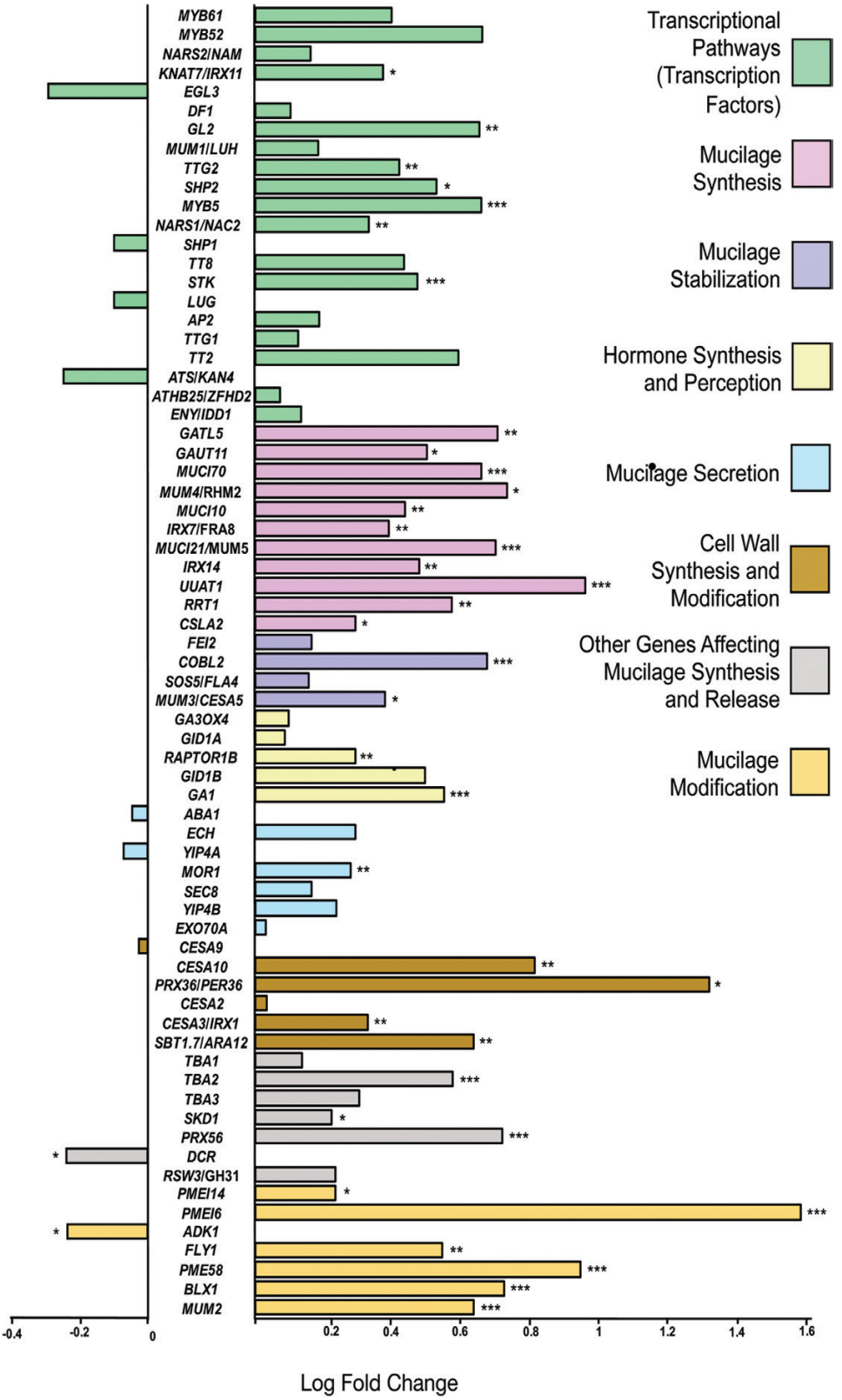

Fig. 3. Relative expression of specific mucilage genes in wild-type versus the *urgt2-2* mutant line. The log_2FC from the genes described as acting in mucilage-specific processes is presented. From the 75 mucilage-specific genes, 70 genes were detected as being expressed in *urgt2-2* by RNA-seq analysis. *ROH.1*, *MYB23*, *DOF4.2*, *MYB75*, and *URGT2* were omitted from the analysis because of the low transcript accumulation. Statistical differences show misregulated genes with *FDR <0.05, **<0.01, ***<0.01.

composition of mucilage (Table 1) and, as expected, we found that Rha decreased by 25% and 13% in the SM and AM, respectively. No changes were observed in seeds where all mucilage was extracted (naked seeds), indicating that changes in *urgt2-2* were specific for mucilage. The decrease in Rha was accompanied by a reduction in the GalA content of 15%

in the SM and 10% in the AM (Table 1; Supplementary Fig. S2A). Interestingly, we observed changes in other sugars, such as Xyl, which increased 23% in SM and 20% in AM. In addition, Ara increased by 35% in AM but decreased by nearly 60% in SM. Moreover, a small but significant decrease in Fuc was also observed in SM. The decrease in Rha and GalA suggested a decrease in RG-I; thus, we used the antibody INRA-RU1 to assess possible changes in this polymer. Reduced labeling was observed in the AM of *urgt2-2* seeds in comparison with WT Col-0 seeds (Supplementary Fig. S2B), thus providing additional evidence of a reduction of RG-I in the mutant. Since we observed an increase in xylose, we also tested antibodies against xylan and xyloglucan on the imbibed seeds. No signal was detected using LM10 and LM11 (xylan); however, using LM25 (xyloglucan), we could detect a thread pattern that was more evident in the *urgt2-2* mutant compared with the WT Col-0 (Fig. 4). In contrast, the radial wall xyloglucan labeling observed on the epidermal cells in the WT Col-0 was decreased in the mutant. However, the Glc content in the AM of *urgt2-2* did not change, suggesting qualitative but not quantitative changes in xyloglucan in the mutant. Finally, the antibodies against arabinan gave no signal.

Table 1. *Monosaccharide composition of adherent and soluble mucilage layers extracted from wild-type and* urgt2-2 *dry seeds*

Sugars	WT Col-0	*urgt2-2*
Soluble mucilage (mg g^{-1} of dry seeds)		
Gal-A	11.87 (0.43)	10.13 (045)**
Rha	12.70 (0.46)	9.74 (0.45)**
Fuc	1.27 (0.32)	0.51 (0.15)*
Ara	0.25 (0.03)	0.15 (0.01)*
Xyl	0.98 (0.03)	1.21 (0.05)*
Man	0.18 (0.01)	0.16 (0.02)
Gal	0.40 (0.02)	0.38 (0.01)
Glc	0.25 (0.09)	0.20 (0.06)
Glc-A	0.40 (0.06)	0.27 (0.03)
Total sugars (SM)	**28.30 (1.52)**	**22.74 (1.07)****
Adherent mucilage (mg g^{-1} of dry seeds)		
Gal-A	5.36 (0.25)	4.84 (0.21)**
Rha	6.06 (0.27)	5.36 (0.28)**
Fuc	0.15 (0.01)	0.15 (0.01)
Ara	0.14 (0.01)	0.19 (0.01)**
Xyl	0.62 (0.03)	0.75 (0.03)***
Man	0.23 (0.01)	0.23 (0.01)
Gal	1.00 (0.04)	1.02 (0.05)
Glc	3.06 (0.38)	2.93 (0.55)
Glc-A	0.14 (0.002)	0.14 (0.004)
Total sugars (AM)	**16.76 (0.46)**	**15.61 (0.62)***
Total sugars (AM+SM)	**45.48 (1.14)**	**38.48 (1.24)****
Total sugars (AM+SM) (%)	**100 (2.51)**	**84.60 (2.72)**
Naked seeds (mg g^{-1} of AIR)		
Gal-A	17.23 (1.72)	16.09 (1.86)
Rha	14.56 (0.99)	14.59 (1.18)
Fuc	2.41 (0.17)	2.23 (0.18)
Ara	25.38 (1.13)	24.05 (1.31)
Xyl	15.60 (1.05)	14.99 (1.21)
Man	4.08 (1.05)	3.99 (0.29)
Gal	24.21 (1.53)	23.73 (1.81)
Glc-A	2.04 (0.13)	2.03 (0.18)
Total sugars	**105.51 (6.73)**	**101.59 (7.84)**

To analyze monosaccharide composition, water and sonication extractions were used to obtain the soluble (SM) and adherent (AM) mucilage, respectively. Sugar content was quantified using HPAEC-PAD from SM, AM, and naked seeds. Means were calculated with data from four biological replicates. SEs are shown in parentheses for two technical replicates each. Asterisks indicate significant statistical differences using Wilcoxon test (* $P<0.05$; ** $P<0.01$, *** $P<0.001$).

The mutation in URGT2 *affects homogalacturonan methylesterification in mucilage*

The transcriptome analysis showed a number of changes in the abundance of transcripts encoding genes involved in modulating pectin methylesterification, such as *PMEI6*, *PMEI14*, *PME58*, *FLY*, and *SBT1.7* (Fig. 3), suggesting that methylesterification of polysaccharides may be different in the mutant; thus, we assessed the global PME activity of dry seed, measured the methanol release in both mucilage layers, and investigated HG methylation in the AM layer by immunolabeling. The results showed that *urgt2-2* had a decrease by 14% in global PME activity in comparison with the WT Col-0 (Fig. 5A) Consistent with the higher PME activity, an increase in methanol released from both layers of mucilage was observed in the *urgt2-2* mutant (Fig. 5B). Immunolabeling of the AM layer using JIM7 and JIM5, which recognize highly and partially methylesterified HG, respectively (Fig. 5C), showed an increase of the JIM7 labeling localized in the external AM (yellow) and a decrease in JIM5 labeling (green). Altogether, these results indicate that mucilage from *urgt2-2* exhibits higher levels of HG methylesterification.

Most NSTs are expressed during mucilage formation

Recently evidence was provided that the absence of the UUAT1 transporter produces pleiotropic changes in mucilage (Saez-Aguayo *et al.*, 2017). Due to the changes observed in sugar content in *urgt2-2*, we decided to investigate whether other NST members could compensate for the lack of *URGT2*. The transcriptomic analysis revealed that 41 out of the 44 putative NSTs described to date are expressed in developing seed at 8 DAP of *urgt2-2*, and 17 were significantly up-regulated in the mutant; whereas one was down-regulated (Fig. 6). The increase in NST expression suggested that NSTs play a role in mucilage biosynthesis to compensate for the lack of URGT2 (Fig. 6). Interestingly, among the six URGTs, only the transcript accumulation of *URGT4* was more abundant in the mutant than in the WT Col-0. Among the up-regulated NSTs, we found four out of the five members of the uronic acid transporters (*UUAT1*, *UUAT3*, *UUAT4*, and *UUAT5*, Rautengarten *et al.*, 2014), three out of the four UDP-Ara*f* transporters (*UAFT2*, *UAFT3*, and *UAFT4,* Rautengarten *et al.*, 2017), and also the UDP-Xyl transporter *UXT3* (Ebert *et al.*, 2015). The analysis of expression of these NST genes on the seed coat, using the data available on the the Arabidopsis eFP Browser platform (Supplementary Fig. S4), revealed that *UUAT1*, *UUAT3*, and *UAFT2* were the three genes with the highest expression in the linear cotyledon stage, which has been described as the stage where mucilage is actively synthesized (Western *et al.*,

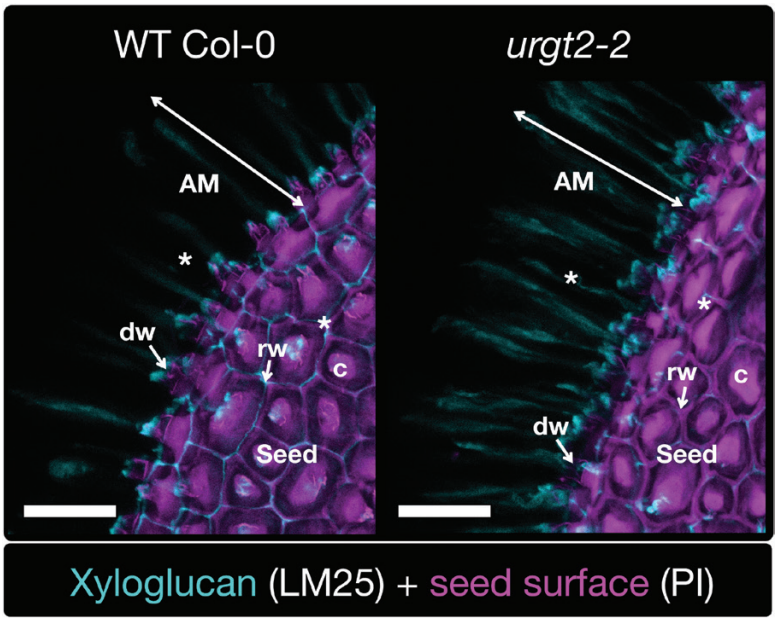

Fig. 4. The *urgt2-2* mutants exhibit a higher labeling of xyloglucan domains in the adherent mucilage (AM) layer. Xyloglucan labeling in AM from imbibed seeds of the WT Col-0 and the *urgt2-2* mutant lines. Confocal microscopy optical section reconstruction of AM released from imbibed seeds. Asterisks represent differences in labeling. LM25 antibody (cyan) was used to label xyloglucan and propidium iodide (PI) was used to detect the seed surface (purple). dw, distal wall; rw; radial walll and c, columella. Scale bar=50 μm.

2000). Therefore, these results suggest that these NST genes may play a role during mucilage biosynthesis.

Assessing the role of NSTs differentially expressed in urgt2-2 *in the biosynthesis of mucilage*

The transcriptome analysis showed that *UUAT1*, *UUAT3*, and *UAFT2* are highly expressed in the mutant. In order to confirm that this up-regulation occurs on both allelic lines, we assessed the transcript levels of both *UUAT3* and *UAFT2* in *urgt2-1* and *urgt2-2*, and they were higher than in the WT Col-0 with the exception of *UAFT2* in *urgt2-2* where we could not see statistical differences from the WT Col-0 (Supplementary Fig. S5A, B). We already know that mutants in *UUAT1* have a mucilage phenotype (Saez-Aguayo *et al.*, 2017); therefore, to determine if *UUAT3* and *UAFT2* are also involved in mucilage formation, we identified two mutant alleles for *UAFT2* (*uaft2-1* and *uaft2-2*) and one mutant allele for *UUAT3* (*uuat3-1*). Since we could not identify more knockout mutants for *UUAT3*, a molecular rescue of *uuat3-1* by transforming this mutant with the *proUUAT3:UUAT3-GFP* construct was performed. The histochemical analysis of *uaft2* mutants revealed less ruthenium red staining and RG-I labeling in the AM (Fig. 7). These results correlated with the monosaccharide composition measured on SM and AM by HPAEC-PAD in *uaft2* mutants (Fig. 9; Supplementary Table S4). The two *uaft2* mutant lines showed a reduction of almost all monosaccharides in the AM layer, which led to a reduction of 17.9% and 20% of total monosaccharide content for *uaft2-1* and *uaft2-1*, respectively. The content of arabinose was significantly reduced in AM (35.3% and 55.3% in *uaft2-1* and *uaft2-2*, respectively) (Fig. 9). Interestingly, no change in Ara was observed in SM; however, a slight increase in Rha and GalA was observed in SM. Furthermore, an increase of 15.7% and 18.9% in the total monosaccharide content of the SM fraction in *uaft2-1* and *uaft2-2*, respectively, has also been observed.

In the case of *uuat3-1*, a higher intensity of ruthenium red staining and stronger RG-I labeling on the AM layer were observed (Fig. 8B, C). Three rescued lines showed ruthenium red staining and RG-I labeling similar to the WT Col-0 confirming that the phenotype was due to the lack of *UUAT3*. Further biochemical analysis of *uuat3-1* revealed that the mutant had a reduction of 20.1% of the total monosaccharide content in the SM layer. This reduction was mainly due to a reduction in Rha, GalA, and Xyl (Fig. 9; Supplementary Table S5). However, no significant changes of total monosaccharide content of the AM layer were observed in the *uuat3* mutant, although there was a slight increase in the content of GalA, Xyl, and Gal.

Discussion

URGT2 is a UDP-rhamnose/UDP-galactose transporter gene involved in the biosynthesis of mucilage RG-I (Rautengarten *et al.*, 2014). A deficiency in this gene produces changes in the content of monosaccharides in mucilage, suggesting that adaptation mechanisms are triggered in the mutant. In order to analyze the changes that take place in the mutant, we performed a transcriptomic analysis of the *urgt2-2* mutant in developing seeds using RNA-seq. We are aware that changes in transcript abundance do not necessarily represent changes in the protein content; however, certainly it is an excellent approach to obtain an overview of the changes triggered in a mutant. Transcriptomic data of *urgt2-2* seeds revealed a misregulation of 3149 genes, a rather large number of genes in comparison with the numbers obtained in recent studies addressing changes in the transcriptome of mutants in genes involved in cell wall metabolism (Guénin *et al.*, 2017;

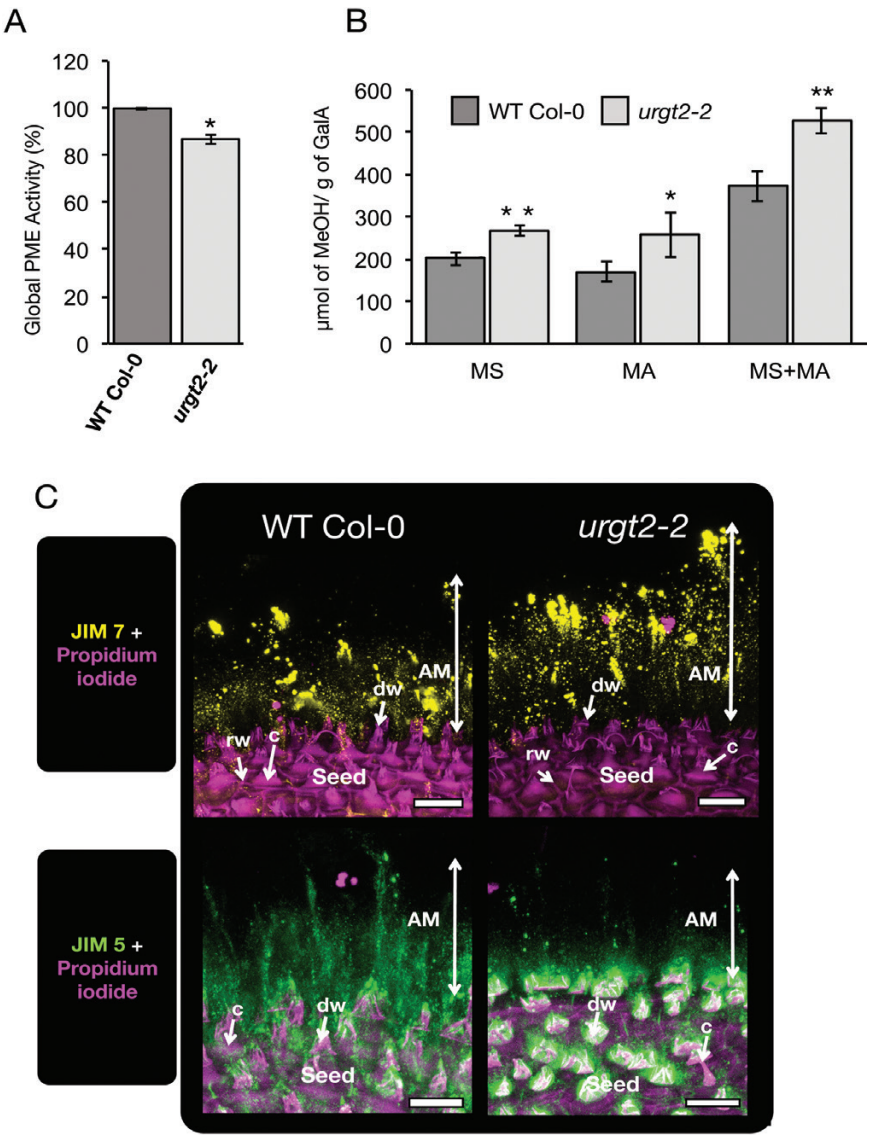

Fig. 5. The *urgt2-2* mutant is reduced in pectin methylesterase (PME) activity and has increased mucilage methylesterification. (A) Global seed PME activity. Total protein extracts from mature dry seeds of the WT Col-0 and *urgt2-2* were used to measure global PME activity. The PME activity was normalized to the average WT Col-0 activity (100%). Error bars represent the SE (n=20 from four biological replicates). Asterisks indicate significant statistical differences using t-test (* P<0.01). (B) Methanol content in the WT Col-0 and *urgt2-2* in adherent and soluble mucilage fractions. Error bars represent the SE (n=20, from four biological replicates). Asterisks indicate significant statistical differences using t-test (*P<0.05, **P<0.01). (C) Homogalacturonan labeling in adherent mucilage from dry seeds of the WT Col-0 and the *urgt2-2* mutant line. Confocal microscopy optical section reconstruction of AM released from imbibed seeds.#8232;JIM7 (yellow) and JIM5 (green) antibodies were used to label highly methylesterified and poorly methylesterified HG domains, respectively. Propidium iodide was used to detect the seed surface (purple). dw, distal cell wall; rw, radial cell wall; and c, columella: scale bar=50 µm.

Faria-Blanc *et al*., 2018). The analysis of mutants in genes involved in secondary cell wall metabolism found few changes in the transcriptome probably due to the fact that cells producing thickening of the secondary cell entered into a cell death program (Faria-Blanc *et al*., 2018). In contrast, the tissue used in this study for the transcriptomic analysis corresponds to seeds from 8 DAP, which are actively developing and engaged in producing large amounts of mucilage. A different study, comparing the transcriptome of a mutant on *AtPME3* and the wild-type showed misregulation in 464 genes (Guénin *et al*., 2017). The transcriptome analysis was performed in etiolated hypocotyls, a tissue that also might be less complex in terms of gene expression than 8 DAP developing seeds. On the other hand, there are technical aspects that may also contribute to explain the differences between our study and those looking for changes in the transcriptome of mutants in other cell wall genes. This is the approach utilized to collect the transcriptomic data, since we used RNA-seq, whereas the other studies used microarray approaches. In fact, this was also the case for a recent study, where the transcriptome analysis of the *mur3* mutant performed by digital gene expression analysis (DGE-seq) revealed the misregulation of 1423 genes (Xu *et al*., 2017). Finally, it is important to highlight that knocking out a single gene leads to an unexpected change in the transcriptome. Whether this is because a change in RG-I or other rhamnosylated molecule needs to be well compensated, or the imbalance in the cellular pools of UDP-Rha triggers this response, remains to be answered.

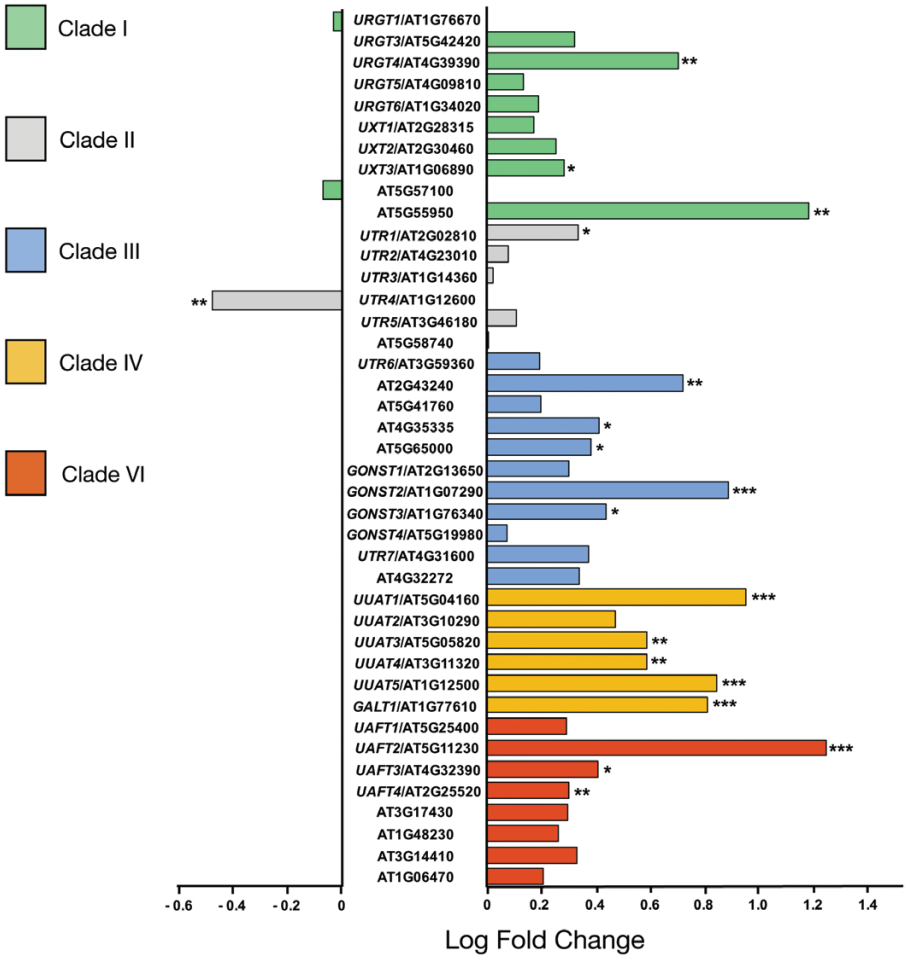

Fig. 6. Nucleotide sugar transporter (NST) expression in the *urgt2-2* mutant line in comparison with the wild-type. The log_2FC from the NST genes is shown. The NST clades are indicated as described by Rautengarten *et al.* (2014). From the 44 NSTs genes, 41 genes were detected as being expressed in the *urgt2-2* RNA-seq analysis. *URGT2*, *GONST5*, and *At1g53660* were omitted from the analysis because of the low transcript accumulation. The triose phosphate clade is not shown. Statistical differences show misregulated genes with *FDR <0.05, **<0.01, ***<0.01.

Since we were interested in the identification of networks that may be related to the function of URGT2, which provides one of the substrates for the synthesis of RG-I, the most abundant polysaccharide in mucilage, we focused our attention on misregulated genes that are related to cell wall metabolism. This analysis was combined with the biochemical and morphological characterization of mucilage.

The mucilage reduction of *urgt2-2* mutants was mainly due to a decrease in the content of Rha and GalA in both the AM and SM layers. Since URGT2 does not transport UDP-GalA, it is likely that the decrease in GalA could be due to an impairment in the synthesis of the RG-I backbone, which is composed of repeating disaccharide units $(GalA–Rha)_n$. A similar phenomenon is observed in a mutant in the UDP-uronic acid transporter 1 (*UUAT1*) described in Saez-Aguayo *et al.* (2017), where a decrease in Rha is associated with a concomitant reduction in GalA. These results indicate that both UUAT1 and URGT2 are involved in the biosynthesis of RG-I, and the lack of either of these transporters leads to a decrease in both sugars in RG-I. Moreover, there have been three genes described which are responsible for the formation of mucilage RG-I, rhamnosyltranferase 1 (*RRT1*) and two putative galacturonosyltransferases, *GATL5* and *MUCI70* (Kong *et al.*, 2013; Takenaka *et al.*, 2018; Voiniciuc *et al.*, 2018). These three genes were up-regulated in the *urgt2-2* seed transcriptome (Fig. 3); however, while qRT-PCR analysis for *GATL5* confirmed this finding, the result for *RRT1* was not conclusive in support of a higher content of *RRT1* in *urgt2-2* (Supplementary Fig. S5C, D). Despite this finding, the overall results tend to support the idea that the RG-I biosynthetic machinery is up-regulated in *urgt2-2*, suggesting that the decrease of UDP-Rha availability could be a limiting factor in the synthesis of this polymer.

Other changes were observed in mucilage from *urgt2-2* plants, which are difficult to reconcile with an impairment in the transport of UDP-Rha. For instance, seeds from the mutant accumulated more Ara and Xyl in the AM layer, while the SM layer showed a strong increase in the content of Xyl, but also a decrease in the content of Fuc and Ara. It has been described that mucilage is composed of low amounts of heteroxylans and xyloglucan (Voiniciuc et al., 2015*b*, *c*). However, the increase in Xyl content on both mucilage layers of *urgt2-2* was not accompanied by an increase of the Glc content, suggesting that *urgt2-2* mucilage did not accumulate xyloglucan and instead this change could be explained by an increase in xylan. Surprisingly, seeds from *urgt2-2* showed higher labeling of xyloglucan epitopes in the adherent mucilage, which could be explained by more

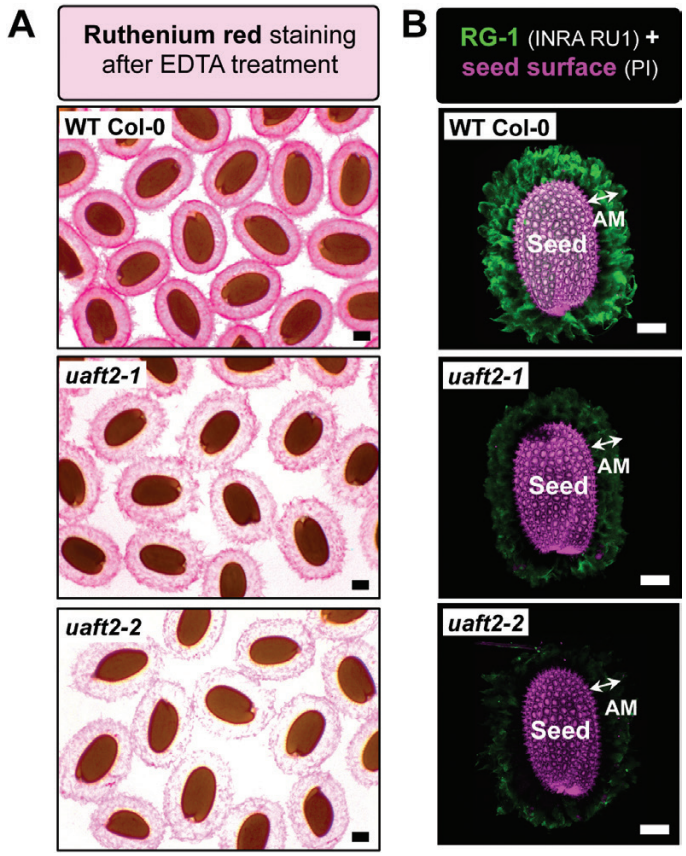

Fig. 7. *uaft2* mutants exhibit an altered adherent mucilage (AM) phenotype. (A) Ruthenium red staining of the AM phenotype in seeds of *uaft2-1* and *uaft2-2* in comparison with the WT Col-0. Seeds were imbibed for 1 h in 0.5 M EDTA and stained with ruthenium red (0.01%). Scale bar=100 μm. (B) Rhamnogalacturonan-I (RG-I) labeling in adherent mucilage from WT Col-0 seeds and the *uaft2* mutant lines. Confocal microscopy optical section reconstruction of AM released from imbibed seeds. INRA RU1 antibody (green) was used to label RG-I epitopes, and propidium iodide was used to stain the seed surface (purple). Scale bar=100 μm.

accessible xyloglucan epitopes on the *urgt2-2* mucilage due to a reduction in the monosaccharide content in this layer. The accumulation of xylose in the AM layer correlated with the up-regulation in the mutant seeds of *UXS3* (Kuang *et al.* 2016) and *UXT3* (Ebert *et al.*, 2015), genes involved in the biosynthesis and transport of UDP-Xyl into the Golgi. Moreover, the increase in *urgt2-2* of transcripts from *IRX14* and *MUCI21*, two putative xylosyltransferase genes that are essential for xylan elongation and substitution in the seed coat mucilage (Voiniciuc *et al.*, 2015*c*), support the idea that the increase in Xyl is due to an accumulation of mucilage xylans. In fact, xylan domains have been proposed as mucilage stabilizers due to their high affinity for cellulose and are involved in RG-I attachments to the mucilage cellulose fibers (Voiniciuc *et al.*, 2015*c*; Ralet *et al.*, 2016); thus, the changes observed in *urgt2-2* may seek a higher stabilization of mucilage in the mutant.

The *urgt2-2* mutant also exhibited changes in the content of Ara, which was slightly higher in the AM and lower in the SM layer in comparison with the wild-type. However, the total content of Ara in mucilage was not altered, with a mean of 0.37 (SD±0.03) mg g^{-1} of seeds for WT Col-0 versus 0.38 (SD±0.03) for mg g^{-1} of seeds for *urgt2-2*, suggesting changes in the partitioning of arabinans between mucilage layers. The increase in arabinans in the AM could be explained by the up-regulation of the UDP-Ara transporter group (*UAFT2*, *UAFT3*, and *UAFT4*; Rautengarten *et al.*, 2017) and higher levels of the *BXL1* transcript, which codes for a bifunctional β-D-xylosidase/α-L-arabinofuranosidase, an enzyme necessary to modify the arabinan present in seed mucilage (Arsovski *et al.*, 2009), and also the putative arabinosyltransferase *RRA1* (Supplementary Table S4), which has been associated with the synthesis of an Ara-containing polymers such as arabinogalactan proteins (AGPs), which may be in close association with cellulose fibers present in the AM (Egelund *et al.*, 2008). Indeed, it could not be discarded that AGPs could have a role in maintaining the adherence of seed mucilage. In the past few years, it has been described that the AGP protein SOS5/FLA4 played a role in mucilage adherence of Arabidopsis seeds (Harpaz-Saad et al., 2011; Griffiths *et al.*, 2014, 2017). However, *SOS5/FLA4* was not significantly misregulated in our RNA-seq study, but, as the authors suggested, other AGPs could also play a role in seed mucilage adherence (Griffiths *et al.*, 2016). Surprisingly, the analysis of the relative expression of AGPs in *urgt2-2* revealed the misregulation of 21 AGP genes from the 151 already described (Ma *et al.*, 2017), 16 of which are up-regulated (Supplementary Table S3). Interestingly, among the *urgt2-2* up-regulated AGPs, ARABINOXYLAN PECTIN ARABINOGALACTAN 1 (APAP1) has been proposed as a candidate to participate in the control of seed mucilage adherence (Höfte, 2015).

The transcriptomic analysis of *urgt2-2* revealed the overexpression of 17 NSTs. Among them, UUAT3 and *UAFT2* were NST genes that are the most highly expressed in seed coat cells. Given this feature and to investigate further the possible role of these NSTs in mucilage formation, we decided to study the mucilage obtained from mutant seeds. The study on *uuat3* revealed a decrease in the content of Rha and GalA in SM, similar to what was already observed in *uuat1* (Saez-Aguayo *et al.*, 2017), indicating that *UUAT3* plays a role in mucilage biosynthesis. In contrast, the content of Rha did not change significantly, whereas GalA had a minor increase in the AM in *uuat3*, suggesting no changes in the content of RG-I in this portion of the mucilage and a slight increase in HG. Interestingly, greater staining with ruthenium red was observed in the AM in *uuat3*, as well as higher immunodetection with the anti-RG-I antibody. The most likely explanation for these results is a higher exposure to carboxyl groups, thus leading to an increased ruthenium red staining. This change could also be responsible for an increase in the immunoreactivity of the anti-RG-I antibody, producing greater labeling in the AM. The activity of UUAT3 has not been assessed yet, but, given the close sequence similarity to UUAT1 and the decrease in GalA, it is likely that it may also transport UDP-uronic acids. In the case of *uaft2* mutants, both allelic lines exhibited a reduction in the content of Ara in the AM. In addition, we observed changes in the distribution of RG-I between the mucilage layers, being less abundant in AM and more abundant in SM. Furthermore, it seemed that the reduction of Ara in the AM of *uaft2* mutants led to the accumulation of a more soluble RG-I in seed coat mucilage, reinforcing the hypothesis that Ara-containing

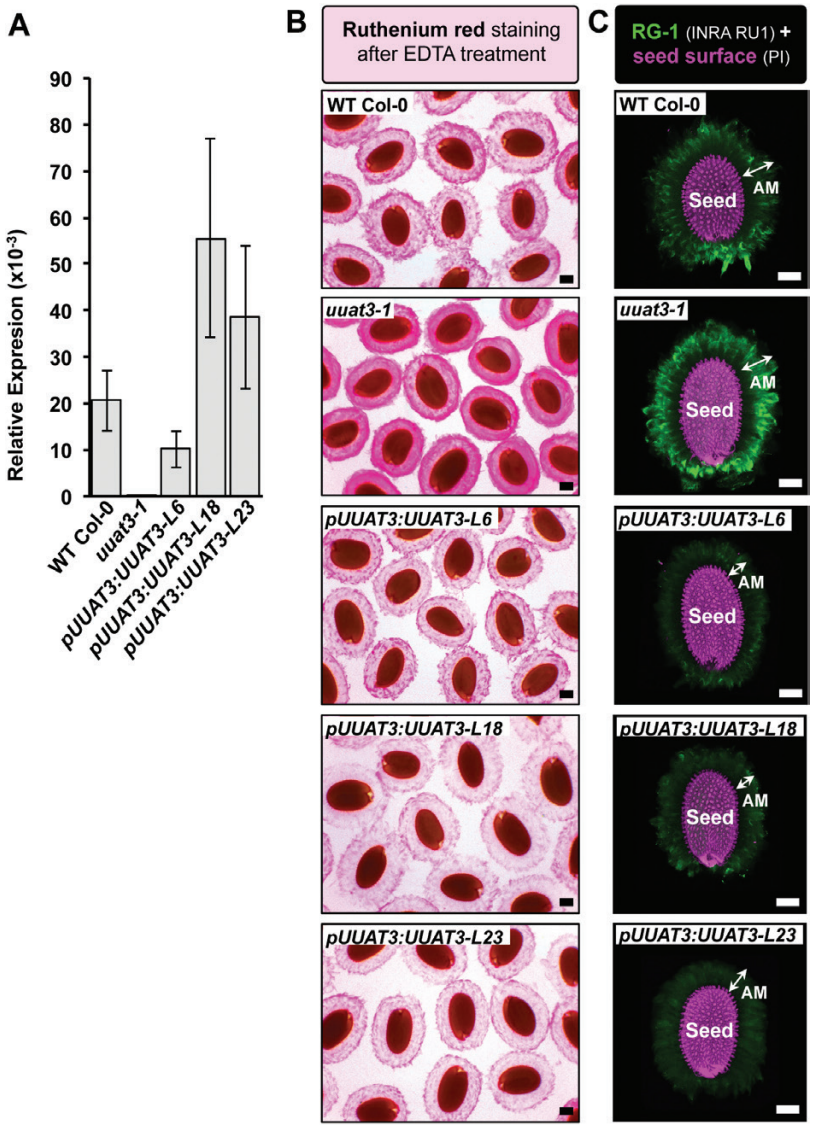

Fig. 8. Molecular rescue of the *uuat3-1* mutant mucilage phenotype using the *proUUAT3:UUAT3-GFP* construct. (A) Expression of *UUAT3* in the *uuat3-1* mutant and the molecular rescue lines. Determination of *UUAT3* mRNA steady state in three *uuat3-1* rescue lines (*proUUAT3:UUAT3*-GFP-L6, -L18, and -L23). The expression was normalized in relation to *EF1αA4* expression. Error bars represent SE values from three biological replicates (n=9). (B) The Ruthenium red adherent mucilage (AM) phenotype is restored in T_3 seeds of three independent *uuat3-1* transformant lines expressing the *UUAT3* CDS fused to GFP under the control of the *UUAT3* promoter (*proUUAT3:UUAT3-GFP*). Seeds were imbibed for 1 h in 0.5 M EDTA and stained with Ruthenium red (0.01%). *proUUAT3:UUAT3*-L6, L-18, and -L23 lines recovered the wild-type AM staining when compared with the *uuat3-1* mutant. Scale bar=100 μm. (C) Rhamnogalacturonan-I (RG-I) labeling in AM from WT Col-0 seeds and the *uuat3-1* mutant line. Confocal microscopy optical section reconstruction of AM released from imbibed seeds. INRA RU1 antibody (green) was used to label RG-I epitopes, and propidium iodide was used to stain the seed surface (purple). *proUUAT3:UUAT3*-L6, L-18, and -L23 lines restored the *uuat3-1* labeling changes. Scale bar=100 μm.

polymers, probably AGPs, could play a role in mucilage adherence (Harpaz-Saad *et al.*, 2011; Griffiths *et al.*, 2014, 2017).

Another important change observed in the *urgt2-2* mutant mucilage was the methylation of HG. Similar to what was described previously in the study on *UUAT1* (Saez-Aguayo *et al.*, 2017), *urgt2-2* dry seed presented a decrease of global PME activity accompanied by an increase in methylesterification. These observations suggest that the reduction of RG-I observed in both *UUAT1* and *URGT2* mutants triggers a compensation mechanism that led to pleiotropic changes in HG methylation (Saez-Aguayo *et al.*, 2017). The phenotype related to changes in HG methylation correlated with the misregulation of genes that have been proposed to be directly involved in the control of HG methylesterification: *PMEI6*, *PMEI14*, *PME52*, *FLY1*, and *SBT1.7* (Rautengarten *et al.*, 2008; Saez-Aguayo *et al.*, 2013; Voiniciuc *et al.*, 2013; Turbant *et al.*, 2016; Shi *et al.*, 2018). Recently, it has been proposed that the transcription factor gene *MYB*52 activates the expression of *PMEI6*, *PMEI14*, and *SBT1.7* (Shi *et al.*, 2018). Surprisingly, the expression of *MYB52* was not significantly changed in *urgt2-2* in comparison with the wild-type. However, *PMEI6*, *PMEI14*, and *SBT1.7* were up-regulated in *urgt2-2*. These results indicated that the mucilage modification and stabilization seemed to be controlled by a complex network regulated by transcription factors (Bui *et al.*, 2011; Huang *et al.*, 2011; Saez-Aguayo *et al.*, 2013; Francoz *et al.*, 2015; Ezquer *et al.*, 2016; Golz *et al.*, 2018;

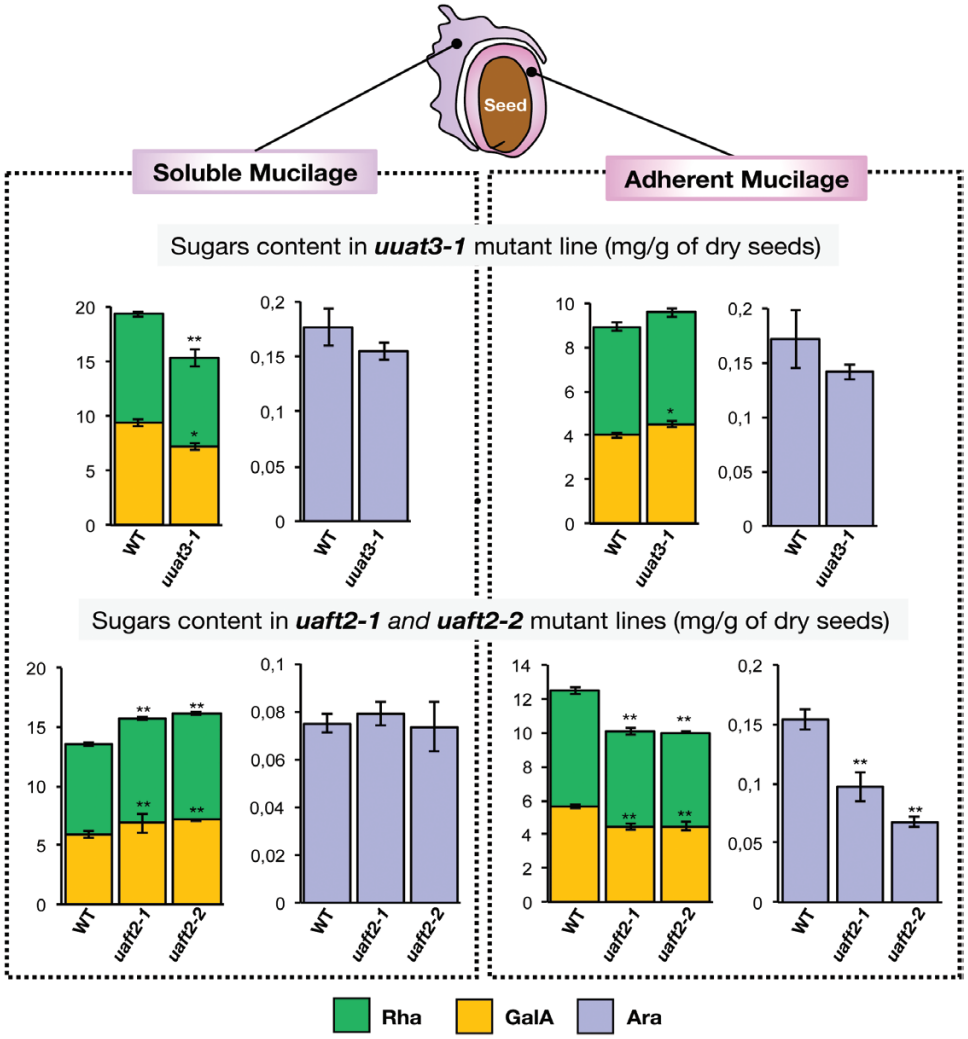

Fig. 9. Mucilage phenotype of *urgt3* and *uaft2* mutant lines. GalA, Rha, and Ara content in soluble (left) and adherent (right) mucilage of *uuat3-1*, *uaft2-1*, and *uaft2-2* T-DNA mutant lines in comparison with their WT Col-0. Sugar content was obtained using HPAEC-PAD from soluble and adherent mucilage. Error bars represent the SE (n=8–12) from 2–3 biological replicates. Asterisks indicate significant statistical differences by Wilcoxon test (*P<0.05; **P<0.01).

Shi *et al.*, 2018). This hypothesis was further strengthened by the finding in the *urgt2-2* mutant line of the up-regulation of the transcription factor genes, which have been previously related to the control of the seed coat formation, *TTG2*, *GL2*, *SHP2*, *NARS/NAC2*, *MYB5*, and *STK* (Western *et al.*, 2000; Windsor *et al.*, 2000; Johnson *et al.*, 2002; Li *et al.*, 2009; Francoz *et al.*, 2015; Ehlers *et al.*, 2016; Ezquer *et al.*, 2016; Tsai *et al.*, 2017). Indeed, it has been reported that the *STK* transcription factor gene positively regulates the expression of *PMEI6* and represses the expression of *SBT1.7* (Ezquer *et al.*, 2016), suggesting the participation of *STK* in the control of HG methylesterification Moreover, the up-regulation of *PMEI6* and *PME14*, both genes coding for PME inhibitors involved in the regulation of mucilage PME activity (Saez-Aguayo *et al.*, 2013; Shi *et al.*, 2018), correlated with the reduction in PME activity and the concomitant reduction in HG methylesterification in *urgt2-2* (Fig. 5). In addition, six putative PMEs were found to be down-regulated in *urgt2-2*, suggesting that they are good candidates to control the HG methylesterification in the seed mucilage of Arabidopsis (Supplementary Table S2). Finally, *urgt2-2* seeds exhibited an up-regulation of *PME58*, a PME gene which has been related to the control of the distribution of HG in the adherent mucilage (Turbant *et al.*, 2016). The overexpression of *PME58* could not correlate with the global PME activity in the *urgt2-2* mutant, but it had been reported that PME58 could be the target for PMEI6, SBT1.7, and FLY1 (Turbant *et al.*, 2016), all of them overexpressed in *urgt2-2*; thus, this finding suggested that the inhibition of PME58 may result in an up-regulation of its expression.

The observation of pleiotropic changes in HG methylesterification in *urgt2-2* is similar to that in mucilage from *uuat1* seeds (Saez-Aguayo *et al.*, 2017), where a mucilage phenotype is also observed; thus, these results suggest the triggering of compensatory mechanisms aiming to maintain the functional integrity of the cell wall (Hamann, 2015*a*, 2015*b*; Höfte, 2015; Voxeur and Höfte, 2016; Chebli and Geitmann, 2017; Bacete *et al.*, 2018). Detection of an altered cell wall composition or sensing altered turgor pressure in epidermal cells due to differences in the composition of the mucilage pocket could be recognized by different plasma membrane receptors which can lead to a compensation response (Hamann, 2015*b*; Voxeur and Höfte, 2016; Wolf, 2017). In Arabidopsis, a

family of receptors, RLK1-Like kinases, have been described to be related to the maintenance of the cell wall homeostasis, perception of mechanical changes, cell wall integrity, and the control of cellular growth (Voxeur and Höfte, 2016; Wolf, 2017). Among members of this family are the receptors THESEUS1 (THE1) and FERONIA (FER), which are found as part of protein complexes with the co-receptors LORELEI and LORELEI-LIKE GPI-ANCHORED proteins (Wolf, 2017). Interestingly *THE1*, *FER*, and *LORELEI-LIKE GPI-ANCHORED PROTEIN 2* were overexpressed in the *urgt2-2* mutant, suggesting that they may play a role in the reorganization set up in the mutant. Nevertheless, *LORELEI-LIKE GPI-ANCHORED PROTEIN 1* was not significantly altered and *LORELEI* was not detected (Supplementary Table S8). FER is an important element of the cell wall integrity (CWI) signaling pathway as this receptor activates a rapid alkalinization of the apoplast, which could be a key process in cell wall remodeling, as some enzymes are very sensitive to pH changes, such as the PME activity which has a high pH optimum (Boyer, 2009). Two mechanisms for how FER receptor activated rapid alkalinization of the apoplast have been described. The first one is to activate the rapid alkalinization factor 1 (RALF1) which is itself a receptor for other RALF and RALF-like proteins (Haruta *et al.*, 2014). The second one involves the association of FER with a plasma membrane H^+-ATPase (AHA2), a protein that is believed to be responsible of the alkalinization of the apoplast. In the *urgt2-2* mutant lines, *AHA2* was overexpressed but *RALF1* was no significantly overexpressed. Nevertheless, we found another two members of the RALF protein family (*At4g14020* and *RALF23*) overexpressed in *urgt2-2*.

Another important sensing module controlling cell wall homeostasis is the brassinosteroid (BR) signaling pathway (Höfte, 2015; Voxeur and Höfte, 2016; Wolf, 2017). The BR receptor complex is formed by the leucine-rich repeat RLKs (LRR-RLKs), BRASSINOSTEROID INSENSITIVE 1 (BRI1) and the co-receptor BRI1-associated kinase 1 (BAK1) (Wolf *et al.*, 2012). The BAK1 protein bound to receptor-like protein 44 (RLP44), which plays a role in the integration of the mechanosensing of cell wall changes in a way independent of the BR sensing module (Wolf, 2014). In fact, it has been proposed that RLP44 senses mechanical cell wall changes, triggering the phosphorylation/dephosphorylation cascade of several members of the BR signaling pathway, leading to the dephosphorylation of the BR-responsive transcription factors BRASSINAZOLE-RESISTANT 1 (BZR1) and BRI1-EMS suppressor 1 (BES1/BZR1) (Sun *et al.*, 2010; Yu *et al.*, 2011). Those transcription factors regulate the expression of several BR-responsive genes, including cell wall biosynthetic genes, such as PMEs and expansins (Sun *et al.*, 2010). Our results showed an up-regulation of *BAK1*, *RLP44*, *BZR1*, and *BRI1 like 3* in *urgt2-2* in comparison with the wild-type. As there was no prior evidence of the existence of a CWI signaling network that senses the changes in the mucilage structure and composition, the changes in CWI signaling genes suggest the possible existence of a sensing and monitoring mechanism of the CWI during seed development in order to promote correct epidermal cell elongation and mucilage deposition. Therefore, it seems that small changes in the mucilage composition, due to the lack of *URGT2*, trigger a range of changes in the expression of cell wall/mucilage polymer synthesis and/or modification genes; which, in turn, were highly regulated in a transcriptional way by the CWI signaling cascade. These results show the plasticity of the cell wall which is crucial to maintain the cell wall functionality.

Acknowledgements

This work was supported by FONDECYT 11160787 (to SS-A), 1151335 (to AO), 3170796 (to ALG), 1160584 (to CM), Fondo de Areas Prioritarias-Centro de Regulacion del Genoma-15090007, ECOS-CONICYT C14B02, and AFB 170004 (to AO), and PAI 79170136 to (SS-A). We thank Miriam Barros for her advice and expertise in confocal microscopy. We also thanks Alvaro Miquel and Macarena Bastias for technical assistance with HPAEC analysis and RNA-sequencing.

Author contributions

SS-A, AL-G, and AO designed the research; JPP-R, SS-A, JC, AL-G, DS, and HT performed the experiments; TC and CM performed informatics analysis; SS-A, JPP-R, AL-G, and AO analyzed the data; and SS-A, AL-G, FCR, and AO wrote the article.

References

Alonso JM, Stepanova AN, Leisse TJ, *et al*. 2003. Genome-wide insertional mutagenesis of *Arabidopsis thaliana*. Science **301**, 653–657.

Anders S, Pyl PT, Huber W. 2015. HTSeq—a python framework to work with high-throughput sequencing data. Bioinformatics **31**, 166–169.

Arabidopsis Genome Initiative. 2000. Analysis of the genome sequence of the flowering plant *Arabidopsis thaliana*. Nature **408**, 796–815.

Arsovski AA, Haughn GW, Western TL. 2010. Seed coat mucilage cells of *Arabidopsis thaliana* as a model for plant cell wall research. Plant Signaling & Behavior **5**, 796–801.

Arsovski AA, Popma TM, Haughn GW, Carpita NC, McCann MC, Western TL. 2009. *AtBXL1* encodes a bifunctional beta-D-xylosidase/alpha-L-arabinofuranosidase required for pectic arabinan modification in Arabidopsis mucilage secretory cells. Plant Physiology **150**, 1219–1234.

Bacete L, Mélida H, Miedes E, Molina A. 2018. Plant cell wall-mediated immunity: cell wall changes trigger disease resistance responses. The Plant Journal **93**, 614–636.

Bakker H, Routier F, Oelmann S, Jordi W, Lommen A, Gerardy-Schahn R, Bosch D. 2005. Molecular cloning of two Arabidopsis UDP-galactose transporters by complementation of a deficient Chinese hamster ovary cell line. Glycobiology **15**, 193–201.

Baldwin TC, Handford MG, Yuseff MI, Orellana A, Dupree P. 2001. Identification and characterization of GONST1, a Golgi-localized GDP-mannose transporter in Arabidopsis. The Plant Cell **13**, 2283–2295.

Barnes WJ, Anderson CT. 2018. Release, recycle, rebuild: cell-wall remodeling, autodegradation, and sugar salvage for new wall biosynthesis during plant development. Molecular Plant **11**, 31–46.

Bar-Peled M, O'Neill MA. 2011. Plant nucleotide sugar formation, interconversion, and salvage by sugar recycling. Annual Review of Plant Biology **62**, 127–155.

Bischoff V, Cookson SJ, Wu S, Scheible WR. 2009. Thaxtomin A affects CESA-complex density, expression of cell wall genes, cell wall composition, and causes ectopic lignification in *Arabidopsis thaliana* seedlings. Journal of Experimental Botany **60**, 955–965.

Bonin CP, Potter I, Vanzin GF, Reiter WD. 1997. The MUR1 gene of *Arabidopsis thaliana* encodes an isoform of GDP-D-mannose-4,6-dehydratase, catalyzing the first step in the de novo synthesis of GDP-L-fucose. Proceedings of National Academy of Science, USA **94**, 2085–2090.

Boyer JS. 2009. Cell wall biosynthesis and the molecular mechanism of plant enlargement. Functional Plant Biology **36**, 383–394.

Bui M, Lim N, Sijacic P, Liu Z. 2011. LEUNIG_HOMOLOG and LEUNIG regulate seed mucilage extrusion in Arabidopsis. Journal of Integrative Plant Biology **53**, 399–408.

Burton RA, Gibeaut DM, Bacic A, Findlay K, Roberts K, Hamilton A, Baulcombe DC, Fincher GB. 2000. Virus-induced silencing of a plant cellulose synthase gene. The Plant Cell **12**, 691–706.

Carpita NC, McCann MC. 2015. Characterizing visible and invisible cell wall mutant phenotypes. Journal of Experimental Botany **66**, 4145–4163.

Chebli Y, Geitmann A. 2017. Cellular growth in plants requires regulation of cell wall biochemistry. Current Opinion in Cell Biology **44**, 28–35.

Dean G, Cao Y, Xiang D, Provart NJ, Ramsay L, Ahad A, White R, Selvaraj G, Datla R, Haughn G. 2011. Analysis of gene expression patterns during seed coat development in Arabidopsis. Molecular Plant **4**, 1074–1091.

Dobin A, Davis CA, Schlesinger F, Drenkow J, Zaleski C, Jha S, Batut P, Chaisson M, Gingeras TR. 2013. STAR: ultrafast universal RNA-seq aligner. Bioinformatics **29**, 15–21.

Du Z, Zhou X, Ling Y, Zhang Z, Su Z. 2010. agriGO: a GO analysis toolkit for the agricultural community. Nucleic Acids Research **38**, W64–W70.

Ebert B, Rautengarten C, Guo X, *et al*. 2015. Identification and characterization of a Golgi-localized UDP-xylose transporter family from Arabidopsis. The Plant Cell **27**, 1218–1227.

Egelund J, Damager I, Faber K, Olsen CE, Ulvskov P, Petersen BL. 2008. Functional characterisation of a putative rhamnogalacturonan II specific xylosyltransferase. FEBS Letters **582**, 3217–3222.

Ehlers K, Bhide AS, Tekleyohans DG, Wittkop B, Snowdon RJ, Becker A. 2016. The MADS box genes ABS, SHP1, and SHP2 are essential for the coordination of cell divisions in ovule and seed coat development and for endosperm formation in *Arabidopsis thaliana*. PLoS One **11**, e0165075.

Ezquer I, Mizzotti C, Nguema-Ona E, *et al*. 2016. The developmental regulator SEEDSTICK controls structural and mechanical properties of the Arabidopsis seed coat. The Plant Cell **28**, 2478–2492.

Faria-Blanc N, Mortimer JC, Dupree P. 2018. A transcriptomic analysis of xylan mutants does not support the existence of a secondary cell wall integrity system in Arabidopsis. Frontiers in Plant Science **9**, 384.

Francoz E, Ranocha P, Burlat V, Dunand C. 2015. Arabidopsis seed mucilage secretory cells: regulation and dynamics. Trends in Plant Science **20**, 515–524.

Gigli-Bisceglia N, Hamann T. 2018. Outside-in control—does plant cell wall integrity regulate cell cycle progression? Physiologia Plantarum **165**, 82–94.

Glusman G, Caballero J, Robinson M, Kutlu B, Hood L. 2013. Optimal scaling of digital transcriptomes. PLoS One **8**, e77885.

Golz JF, Allen PJ, Li SF, Parish RW, Jayawardana NU, Bacic A, Doblin MS. 2018. Layers of regulation—insights into the role of transcription factors controlling mucilage production in the Arabidopsis seed coat. Plant Science **272**, 179–192.

Griffiths JS, Crepeau MJ, Ralet MC, Seifert GJ, North HM. 2016. Dissecting seed mucilage adherence mediated by FEI2 and SOS5. Frontiers in Plant Science **7**, 1073.

Griffiths JS, North HM. 2017. Sticking to cellulose: exploiting Arabidopsis seed coat mucilage to understand cellulose biosynthesis and cell wall polysaccharide interactions. New Phytologist **214**, 959–966.

Griffiths JS, Tsai AY, Xue H, Voiniciuc C, Sola K, Seifert GJ, Mansfield SD, Haughn GW. 2014. SALT-OVERLY SENSITIVE5 mediates Arabidopsis seed coat mucilage adherence and organization through pectins. Plant Physiology **165**, 991–1004.

Guénin S, Hardouin J, Paynel F, *et al*. 2017. AtPME3, a ubiquitous cell wall pectin methylesterase of *Arabidopsis thaliana*, alters the metabolism of cruciferin seed storage proteins during post-germinative growth of seedlings. Journal of Experimental Botany **68**, 1083–1095.

Guénin S, Mareck A, Rayon C, *et al*. 2011. Identification of pectin methylesterase 3 as a basic pectin methylesterase isoform involved in adventitious rooting in *Arabidopsis thaliana*. New Phytologist **192**, 114–126.

Hamann T. 2015*a*. The plant cell wall integrity maintenance mechanism—concepts for organization and mode of action. Plant & Cell Physiology **56**, 215–223.

Hamann T. 2015*b*. The plant cell wall integrity maintenance mechanism—a case study of a cell wall plasma membrane signaling network. Phytochemistry **112**, 100–109.

Handford M, Rodríguez-Furlán C, Marchant L, Segura M, Gómez D, Alvarez-Buylla E, Xiong GY, Pauly M, Orellana A. 2012. *Arabidopsis thaliana* AtUTr7 encodes a Golgi-localized UDP-glucose/UDP-galactose transporter that affects lateral root emergence. Molecular Plant **5**, 1263–1280.

Handford MG, Sicilia F, Brandizzi F, Chung JH, Dupree P. 2004. *Arabidopsis thaliana* expresses multiple Golgi-localised nucleotide-sugar transporters related to GONST1. Molecular Genetics and Genomics **272**, 397–410.

Harpaz-Saad S, McFarlane HE, Xu S, Divi UK, Forward B, Western TL, Kieber JJ. 2011. Cellulose synthesis via the FEI2 RLK/SOS5 pathway and cellulose synthase 5 is required for the structure of seed coat mucilage in Arabidopsis. The Plant Journal **68**, 941–953.

Haruta M, Sabat G, Stecker K, Minkoff BB, Sussman MR. 2014. A peptide hormone and its receptor protein kinase regulate plant cell expansion. Science **343**, 408–411.

Höfte H. 2015. The yin and yang of cell wall integrity control: brassinosteroid and FERONIA signaling. Plant & Cell Physiology **56**, 224–231.

Höfte H, Voxeur A. 2017. Plant cell walls. Current Biology **27**, R865–R870.

Hong SM, Bahn SC, Lyu A, Jung HS, Ahn JH. 2010. Identification and testing of superior reference genes for a starting pool of transcript normalization in Arabidopsis. Plant & Cell Physiology **51**, 1694–1706.

Hu R, Li J, Wang X, Zhao X, Yang X, Tang Q, He G, Zhou G, Kong Y. 2016. Xylan synthesized by irregular Xylem 14 (IRX14) maintains the structure of seed coat mucilage in Arabidopsis. Journal of Experimental Botany **67**, 1243–1257.

Huang J, DeBowles D, Esfandiari E, Dean G, Carpita NC, Haughn GW. 2011. The Arabidopsis transcription factor LUH/MUM1 is required for extrusion of seed coat mucilage. Plant Physiology **156**, 491–502.

Johnson CS, Kolevski B, Smyth DR. 2002. TRANSPARENT TESTA GLABRA2, a trichome and seed coat development gene of Arabidopsis, encodes a WRKY transcription factor. The Plant Cell **14**, 1359–1375.

Kim SJ, Held MA, Zemelis S, Wilkerson C, Brandizzi F. 2015. CGR2 and CGR3 have critical overlapping roles in pectin methylesterification and plant growth in *Arabidopsis thaliana*. The Plant Journal **82**, 208–220.

Knappe S, Flügge UI, Fischer K. 2003. Analysis of the plastidic phosphate translocator gene family in Arabidopsis and identification of new phosphate translocator-homologous transporters, classified by their putative substrate-binding site. Plant Physiology **131**, 1178–1190.

Kong Y, Zhou G, Abdeen AA, *et al*. 2013. GALACTURONOSYLTRANSFERASE-LIKE5 is involved in the production of Arabidopsis seed coat mucilage. Plant Physiology **163**, 1203–1217.

Kuang B, Zhao X, Zhou C, *et al*. 2016. Role of UDP-glucuronic acid decarboxylase in xylan biosynthesis in Arabidopsis. Molecular Plant **9**, 1119–1131.

Levesque-Tremblay G, Pelloux J, Braybrook SA, Müller K. 2015. Tuning of pectin methylesterification: consequences for cell wall biomechanics and development. Planta **242**, 791–811.

Li H, Handsaker B, Wysoker A, Fennell T, Ruan J, Homer N, Marth G, Abecasis G, Durbin R; **1000 Genome Project Data Processing Subgroup**. 2009. The sequence alignment/map format and SAMtools. Bioinformatics **25**, 2078–2079.

Liepman AH, Wightman R, Geshi N, Turner SR, Scheller HV. 2010. Arabidopsis—a powerful model system for plant cell wall research. The Plant Journal **61**, 1107–1121.

Ma Y, Yan C, Li H, Wu W, Liu Y, Wang Y, Chen Q, Ma H. 2017. Bioinformatics prediction and evolution analysis of arabinogalactan proteins in the plant kingdom. Frontiers in Plant Science **8**, 66.

Macquet A, Ralet MC, Loudet O, Kronenberger J, Mouille G, Marion-Poll A, North HM. 2007. A naturally occurring mutation in an Arabidopsis accession affects a beta-D-galactosidase that increases the hydrophilic potential of rhamnogalacturonan I in seed mucilage. The Plant Cell **19**, 3990–4006.

Martin M. 2011. Cutadapt removes adapter sequences from high-throughput sequencing reads. EMBnet. Journal **17**, 10.

Nakagawa T, Kurose T, Hino T, Tanaka K, Kawamukai M, Niwa Y, Toyooka K, Matsuoka K, Jinbo T, Kimura T. 2007. Development of

series of gateway binary vectors, pGWBs, for realizing efficient construction of fusion genes for plant transformation. Journal of Bioscience and Bioengineering **104**, 34–41.

Norambuena L, Marchant L, Berninsone P, Hirschberg CB, Silva H, Orellana A. 2002. Transport of UDP-galactose in plants. Identification and functional characterization of AtUTr1, an *Arabidopsis thaliana* UDP-galactos/UDP-glucose transporter. Journal of Biological Chemistry **277**, 32923–32929.

Norambuena L, Nilo R, Handford M, Reyes F, Marchant L, Meisel L, Orellana A. 2005. AtUTr2 is an *Arabidopsis thaliana* nucleotide sugar transporter located in the Golgi apparatus capable of transporting UDP-galactose. Planta **222**, 521–529.

North HM, De Almeida A, Boutin JP, Frey A, To A, Botran L, Sotta B, Marion-Poll A. 2007. The Arabidopsis ABA-deficient mutant aba4 demonstrates that the major route for stress-induced ABA accumulation is via neoxanthin isomers. The Plant Journal **50**, 810–824.

Orellana A, Moraga C, Araya M, Moreno A. 2016. Overview of nucleotide sugar transporter gene family functions across multiple species. Journal of Molecular Biology **428**, 3150–3165.

Ralet MC, Crépeau MJ, Vigouroux J, Tran J, Berger A, Sallé C, Granier F, Botran L, North HM. 2016. Xylans provide the structural driving force for mucilage adhesion to the Arabidopsis seed coat. Plant Physiology **171**, 165–178.

Ralet MC, Tranquet O, Poulain D, Moïse A, Guillon F. 2010. Monoclonal antibodies to rhamnogalacturonan I backbone. Planta **231**, 1373–1383.

Rasool B, McGowan J, Pastok D, Marcus SE, Morris J, Verrall SR, Hedley PE, Hancock RD. 2017. Redox control of aphid resistance through altered cell wall composition and nutritional quality. Plant Physiology **175**, 259–271.

Rautengarten C, Birdseye D, Pattathil S, **, *et al***. 2017. The elaborate route for UDP-arabinose delivery into the Golgi of plants. Proceedings of National Academy of Sciences, USA **114**, 4261–4266.

Rautengarten C, Ebert B, Liu L, Stonebloom S, Smith-Moritz AM, Pauly M, Orellana A, Scheller HV, Heazlewood JL. 2016. The Arabidopsis Golgi-localized GDP-L-fucose transporter is required for plant development. Nature Communications **7**, 12119.

Rautengarten C, Ebert B, Moreno I, *et al*. 2014. The Golgi localized bifunctional UDP-rhamnose/UDP-galactose transporter family of Arabidopsis. Proceedings of the National Academy of Sciences, USA **111**, 11563–11568.

Rautengarten C, Usadel B, Neumetzler L, Hartmann J, Büssis D, Altmann T. 2008. A subtilisin-like serine protease essential for mucilage release from Arabidopsis seed coats. The Plant Journal **54**, 466–480.

Reyes F, Orellana A. 2008. Golgi transporters: opening the gate to cell wall polysaccharide biosynthesis. Current Opinion in Plant Biology **11**, 244–251.

Ridley BL, O'Neill MA, Mohnen D. 2001. Pectins: structure, biosynthesis, and oligogalacturonide-related signaling. Phytochemistry **57**, 929–967.

Robinson MD, McCarthy DJ, Smyth GK. 2010. edgeR: a Bioconductor package for differential expression analysis of digital gene expression data. Bioinformatics **26**, 139–140.

Rollwitz I, Santaella M, Hille D, Flügge UI, Fischer K. 2006. Characterization of AtNST-KT1, a novel UDP-galactose transporter from *Arabidopsis thaliana*. FEBS Letters **580**, 4246–4251.

Saez-Aguayo S, Ralet MC, Berger A, Botran L, Ropartz D, Marion-Poll A, North HM. 2013. PECTIN METHYLESTERASE INHIBITOR6 promotes Arabidopsis mucilage release by limiting methylesterification of homogalacturonan in seed coat epidermal cells. The Plant Cell **25**, 308–323.

Saez-Aguayo S, Rautengarten C, Temple H, *et al*. 2017. UUAT1 is a Golgi-localized UDP-uronic acid transporter that modulates the polysaccharide composition of Arabidopsis seed mucilage. The Plant Cell **29**, 129–143.

Salem MA, Li Y, Wiszniewski A, Giavalisco P. 2017. Regulatory-associated protein of TOR (RAPTOR) alters the hormonal and metabolic composition of Arabidopsis seeds, controlling seed morphology, viability and germination potential. The Plant Journal **92**, 525–545.

Scheible WR, Pauly M. 2004. Glycosyltransferases and cell wall biosynthesis: novel players and insights. Current Opinion in Plant Biology **7**, 285–295.

Seifert GJ. 2004. Nucleotide sugar interconversions and cell wall biosynthesis: how to bring the inside to the outside. Current Opinion in Plant Biology **7**, 277–284.

Shi D, Ren A, Tang X, Qi G, Xu Z, Chai G, Hu R, Zhou G, Kong Y. 2018. MYB52 negatively regulates pectin demethylesterification in seed coat mucilage. Plant Physiology **176**, 2737–2749.

Shimada T, Kunieda T, Sumi S, Koumoto Y, Tamura K, Hatano K, Ueda H, Hara-Nishimura I. 2018. The AP-1 complex is required for proper mucilage formation in Arabidopsis seeds. Plant & Cell Physiology **59**, 2331–2338.

Sterling JD, Quigley HF, Orellana A, Mohnen D. 2001. The catalytic site of the pectin biosynthetic enzyme alpha-1,4-galacturonosyltransferase is located in the lumen of the Golgi. Plant Physiology **127**, 360–371.

Sun Y, Fan XY, Cao DM, *et al*. 2010. Integration of brassinosteroid signal transduction with the transcription network for plant growth regulation in Arabidopsis. Developmental Cell **19**, 765–777.

Takenaka Y, Kato K, Ogawa-Ohnishi M, *et al*. 2018. Pectin RG-I rhamnosyltransferases represent a novel plant-specific glycosyltransferase family. Nature Plants **4**, 669–676.

Taylor-Teeples M, Lin L, de Lucas M, *et al*. 2015. An Arabidopsis gene regulatory network for secondary cell wall synthesis. Nature **517**, 571–575.

Temple H, Saez-Aguayo S, Reyes FC, Orellana A. 2016. The inside and outside: topological issues in plant cell wall biosynthesis and the roles of nucleotide sugar transporters. Glycobiology **26**, 913–925.

Tsai AY, Kunieda T, Rogalski J, Foster LJ, Ellis BE, Haughn GW. 2017. Identification and characterization of Arabidopsis seed coat mucilage proteins. Plant Physiology **173**, 1059–1074.

Turbant A, Fournet F, Lequart M, Zabijak L, Pageau K, Bouton S, Van Wuytswinkel O. 2016. PME58 plays a role in pectin distribution during seed coat mucilage extrusion through homogalacturonan modification. Journal of Experimental Botany **67**, 2177–2190.

Verhertbruggen Y, Marcus SE, Chen J, Knox JP. 2013. Cell wall pectic arabinans influence the mechanical properties of *Arabidopsis thaliana* inflorescence stems and their response to mechanical stress. Plant & Cell Physiology **54**, 1278–1288.

Voiniciuc C, Dean GH, Griffiths JS, Kirchsteiger K, Hwang YT, Gillett A, Dow G, Western TL, Estelle M, Haughn GW. 2013. Flying saucer1 is a transmembrane RING E3 ubiquitin ligase that regulates the degree of pectin methylesterification in Arabidopsis seed mucilage. The Plant Cell **25**, 944–959.

Voiniciuc C, Engle KA, Günl M, Dieluweit S, Schmidt MH, Yang JY, Moremen KW, Mohnen D, Usadel B. 2018. Identification of key enzymes for pectin synthesis in seed mucilage. Plant Physiology **178**, 1045–1064.

Voiniciuc C, Günl M, Schmidt MH, Usadel B. 2015*a*. Highly branched xylan made by IRREGULAR XYLEM14 and MUCILAGE-RELATED21 links mucilage to Arabidopsis seeds. Plant Physiology **169**, 2481–2495.

Voiniciuc C, Schmidt MH, Berger A, Yang B, Ebert B, Scheller HV, North HM, Usadel B, Günl M. 2015*b*. MUCILAGE-RELATED10 produces galactoglucomannan that maintains pectin and cellulose architecture in Arabidopsis seed mucilage. Plant Physiology **169**, 403–420.

Voiniciuc C, Yang B, Schmidt MH, Günl M, Usadel B. 2015*c*. Starting to gel: how Arabidopsis seed coat epidermal cells produce specialized secondary cell walls. International Journal of Molecular Sciences **16**, 3452–3473.

Voxeur A, Höfte H. 2016. Cell wall integrity signaling in plants: 'To grow or not to grow that's the question'. Glycobiology **26**, 950–960.

Western TL. 2012. The sticky tale of seed coat mucilages: production, genetics, and role in seed germination and dispersal. Seed Science Research. **22,** 1–25.

Western TL, Skinner DJ, Haughn GW. 2000. Differentiation of mucilage secretory cells of the Arabidopsis seed coat. Plant Physiology **122**, 345–356.

Western TL, Young DS, Dean GH, Tan WL, Samuels AL, Haughn GW. 2004. MUCILAGE-MODIFIED4 encodes a putative pectin biosynthetic enzyme developmentally regulated by APETALA2, TRANSPARENT TESTA GLABRA1, and GLABRA2 in the Arabidopsis seed coat. Plant Physiology **134**, 296–306.

Windsor JB, Symonds VV, Mendenhall J, Lloyd AM. 2000. Arabidopsis seed coat development: morphological differentiation of the outer integument. The Plant Journal **22**, 483–493.

Wolf S. 2017. Plant cell wall signalling and receptor-like kinases. The Biochemical Journal **474**, 471–492.

Wolf S, Hématy K, Höfte H. 2012. Growth control and cell wall signaling in plants. Annual Review of Plant Biology **63**, 381–407.

Wolf S, van der Does D, Ladwig F, *et al*. 2014. A receptor-like protein mediates the response to pectin modification by activating brassinosteroid signaling. Proceedings of National Academy of Sciences, USA **111**, 15261–15266.

Wulff C, Norambuena L, Orellana A. 2000. GDP-fucose uptake into the Golgi apparatus during xyloglucan biosynthesis requires the activity of a transporter-like protein other than the UDP-glucose transporter. Plant Physiology **122**, 867–877.

Xu Z, Wang M, Shi D, Zhou G, Niu T, Hahn MG, O'Neill MA, Kong Y. 2017. DGE-seq analysis of MUR3-related Arabidopsis mutants provides insight into how dysfunctional xyloglucan affects cell elongation. Plant Science **258**, 156–169.

Yong W, Link B, O'Malley R, *et al*. 2005. Genomics of plant cell wall biogenesis. Planta **221**, 747–751.

Young RE, McFarlane HE, Hahn MG, Western TL, Haughn GW, Samuels AL. 2008. Analysis of the Golgi apparatus in Arabidopsis seed coat cells during polarized secretion of pectin-rich mucilage. The Plant Cell **20**, 1623–1638.

Yu X, Li L, Zola J, *et al*. 2011. A brassinosteroid transcriptional network revealed by genome-wide identification of BESI target genes in *Arabidopsis thaliana*. The Plant Journal **65**, 634–646.

Zhao X, Qiao L, Wu AM. 2017. Effective extraction of Arabidopsis adherent seed mucilage by ultrasonic treatment. Scientific Reports **7**, 40672.